A Lagrangian Analysis of the Atmospheric Branch of the Global Water Cycle. Part II: Moisture Transports between Earth's Ocean Basins and River Catchments

ANDREAS STOHL

Norwegian Institute for Air Research, Kjeller, Norway

PAUL JAMES*

Technical University of Munich, Munich, Germany

(Manuscript received 12 November 2004, in final form 6 May 2005)

ABSTRACT

A diagnostic Lagrangian method to trace the budgets of freshwater fluxes, first described in Part I of this article, is used here to establish source–sink relationships of moisture between earth's ocean basins and river catchments. Using the Lagrangian particle dispersion model FLEXPART, driven with meteorological analyses, 1.1 million particles, representing the mass of the atmosphere, were tracked over a period of 4 yr. Via diagnosis of the changes of specific humidity along the trajectories, budgets of evaporation minus precipitation ($E - P$) were determined. For validation purposes, $E - P$ budgets were calculated for 39 river catchments and compared with climatological streamflow data for these rivers. Good agreement (explained variance 87%) was found between the two quantities. The $E - P$ budgets were then tracked forward from all of earth's ocean basins and backward from the 39 major river catchments for a period of 10 days. As much previous work was done for the Mississippi basin, this basin was chosen for a detailed analysis. Moisture recycling over the continent and moisture transport from the Gulf of Mexico were identified as the major sources for precipitation over the Mississippi basin, in quantitative agreement with previous studies. In the remainder of the paper, global statistics for source–sink relationships of moisture between the ocean basins and river catchments are presented. They show, for instance, the evaporative capacity of monsoonal flows for precipitation over the Ganges and Niger catchments, and the transport of moisture from both hemispheres to supply the Amazon's precipitation. In contrast, precipitation in northern Eurasia draws its moisture mainly via recycling over the continent. The atmospheric transport of moisture between different ocean basins was also investigated. It was found that transport of air from the North Pacific produces net evaporation over the North Atlantic, but not vice versa. This helps to explain why the sea surface salinity is higher in the North Atlantic than in the North Pacific, a difference thought to be an important driver of the oceans' thermohaline circulation. Finally, limitations of the method are discussed and possible future developments are outlined.

1. Introduction

Transport of water vapor in the atmosphere from regions of net evaporation to regions of net precipitation is an important part of the hydrological cycle. Freshwater falling as precipitation is a valuable resource, and, especially in regions with scarce supply, it is important to know where this resource is coming from (e.g., Gong and Eltahir 1996) because only then is it possible to assess how it responds to hydrological changes in its source region.

Transport of water vapor in the atmosphere is also a driving force of the thermohaline circulation (Weaver et al. 1999). The North Atlantic Ocean, for instance, is a relatively strong source of water vapor through net evaporation, in contrast to the North Pacific Ocean. This leads to a higher sea surface salinity in the North Atlantic than in the North Pacific Ocean. Fresher water flowing through the Bering Strait from the Pacific into the Arctic and North Atlantic Ocean partly compen-

* Current affiliation: Met Office, Exeter, United Kingdom.

Corresponding author address: Andreas Stohl, Department of Regional and Global Pollution Issues, Norwegian Institute for Air Research, P.O. Box 100, N-2027 Kjeller, Norway.
E-mail: ast@nilu.no

sates this, but the higher sea surface salinity is still thought to be an important reason why deep water is formed in the North Atlantic, but not in the North Pacific (Hasumi 2002). It has been speculated that the atmospheric transport of moisture from the subtropics to the higher latitudes is more effective in the North Pacific than in the North Atlantic and thus maintains the northern North Pacific's lower sea surface salinity (Emile-Geay et al. 2003). However, this does not account for atmospheric transport of moisture between the ocean basins, which may also be responsible for the salinity differences between the two oceans.

Moisture transport between different regions of the earth is difficult to quantify as it involves all components of the hydrologic cycle. In the framework of general circulation models, water tracers can be tagged according to the water's source region to evaluate their contribution over receptor regions (Koster et al. 1986; Numaguti 1999; Bosilovich and Schubert 2002; Bosilovich et al. 2003). However, general circulation models have a number of weaknesses (e.g., microphysical parameterizations) regarding their capability to realistically simulate the hydrological cycle. Therefore, there is a need for independent diagnostic methods to quantify moisture transports based on observational or meteorological analysis data. There exist simple diagnostic methods to calculate so-called recycling ratios, the fraction of precipitation that originates locally within a region (Eltahir and Bras 1996). Apart from their sensitivity to the choice of a length scale and their dependence on the assumption of a well-mixed atmosphere, recycling models cannot determine where the water with a nonlocal source is coming from. With other diagnostic methods, such as the mapping of vertically integrated atmospheric moisture fluxes (e.g., Smirnov and Moore 2001; Liu and Stewart 2003), regions of net convergence and divergence of moisture can be determined. But as the atmospheric circulation is not stationary, these maps are misleading regarding the transport of water vapor from its evaporative sources to its precipitation sinks. Integrating the moisture fluxes across a basin boundary (e.g., Chen et al. 1994) allows one to quantify the in- or outflow of moisture to or from a basin, but does not say where the moisture crossing the boundary is coming from or going to. For such transport studies, trajectories have often been applied, either qualitatively in case studies (Crimp and Mason 1999; Bertò et al. 2004; Knippertz and Martin 2005, hereafter KM), or quantitatively involving prognostic evaporation data (Dirmeyer and Brubaker 1999).

This paper applies a new Lagrangian diagnostic method developed in the companion paper to this article (Stohl and James 2004, hereafter Part I). Using meteorological analysis data it determines whether transport of air masses from a source ocean basin causes net evaporation or net precipitation in other ocean basins. It also identifies reasonably strong precipitation events over river basins and answers the question of where the water producing the precipitation came from. The next section briefly reviews the method and describes its application here. Section 3 provides further validation of the method, section 4 gives examples of the moisture tracking, and section 5 presents global statistics of moisture transport between earth's major ocean and river basins. Section 6 discusses strengths and weaknesses of the method and the reliability of the results obtained, and, finally, conclusions are drawn in section 7.

2. Methods

In Part I, we presented a new method to track atmospheric moisture along trajectories calculated using the Lagrangian particle dispersion model FLEXPART (Stohl et al. 1998) driven with meteorological analysis data from the European Centre for Medium-Range Weather Forecasts (ECMWF) (White 2002). A large number of so-called particles was distributed homogeneously in the atmosphere and then transported by the model using the full three-dimensional winds, as resolved in the ECMWF analyses. Their positions were recorded every 3 h together with the specific humidity q interpolated from the ECMWF data. ECMWF moisture analyses are less accurate than mass and momentum analyses, but the analyses are still strongly constrained by humidity measurements. Therefore, changes in the moisture fields from analysis time to analysis time largely reflect real hydrological processes. As many of these processes (e.g., assumptions on subgrid-scale convective fluxes, entrainment, detrainment, condensation, precipitation initiation, etc.) are poorly understood, humidity changes with time are less uncertain than those taken from a free-running model. The extent to which they are constrained by actual observations, however, depends on the accuracy and availability of observations as well as on the quality of the data assimilation.

From the FLEXPART output, changes in q with time t were used to diagnose the moisture budget of a particle,

$$e - p = m\frac{dq}{dt}, \tag{1}$$

where m is the particle's mass, and e and p are the rates of moisture increases and decreases along the trajec-

tory, respectively. It was shown that by solving Eq. (1) for all particles and amassing $e - p$ over all K particles residing in the atmospheric column over an area A,

$$E - P \approx \frac{\sum_{k=1}^{K} (e - p)}{A} \tag{2}$$

is equivalent to the Eulerian budget equation

$$E - P = \frac{\partial w}{\partial t} + \nabla \cdot \frac{1}{g} \int_0^{p_s} q\mathbf{v}\, dp, \tag{3}$$

where $E - P$ is the surface freshwater flux, $w = (1/g)\int_0^{p_s} q\ dp$ is the precipitable water, g is the gravitational acceleration, p_s is the surface pressure, $\mathbf{v}$ is the wind, and E and P are the evaporation and precipitation rates per unit area, respectively (Trenberth and Guillemot 1998). We showed that when using a large enough number of particles, the two methods give almost identical results. Essentially, this method diagnoses a quantity ($E - P$) that is not observed by a global network, from analyzed changes in a quantity (q) that is observed, using also-analyzed wind data.

Under certain assumptions, the method can also separate E and P but it was shown that this separation is ambiguous and results are reasonably accurate only when one of the two terms is known to be much larger than the other, for instance when $P \gg E$ during rain events. For many purposes, for instance the determination of the freshwater budget over the oceans, a separation of E and P is indeed not needed at all. But to identify the water source regions for precipitation over land, we diagnose reasonably strong precipitation events. The main advantage of the Lagrangian method [Eq. (2)] over the Eulerian method [Eq. (3)] is that it can also track $E - P$ from a region forward or backward in time by evaluating Eq. (1) along the trajectories of appropriately selected particles.

The model, FLEXPART version 5.1, and its setup is exactly the same as in Part I and is, therefore, not described here. The only difference to the previous study is that 1.1 million particles, 300 000 more than previously, were used. In addition to advection with the resolved winds, the model also accounts for subgrid turbulence by adding random motion components to the particles (Stohl et al. 1998), which is important especially in the boundary layer. The model's convection scheme was not used in this study. High vertical resolution at low altitudes is important because most of the water vapor resides in the lower troposphere. Because ECMWF increased the vertical resolution of its operational model to 60 levels (of which approximately 14 are below 1500 m and 23 are below 5000 m) in October 1999, we used the period 1 November 1999 to 30 November 2003 for our study. Global indices of climate variability (e.g., the multivariate El Niño–Soutern Oscillation index available from the Climate Diagnostics Center) do not show any extreme values or biased mean values during that period. Thus, the climate conditions during the 4 yr should be rather typical on a global scale.

We used ECMWF operational global analyses every 6 h (at 0000, 0600, 1200, and 1800 UTC), and 3-h forecasts at intermediate times (at 0300, 0900, 1500, and 2100 UTC) with $1^\circ \times 1^\circ$ resolution and all 60 vertical levels. Note that the method could have been used also without the forecast data, the major difference being a somewhat decreased resolution and accuracy because of the long time step. Several changes were made to the operational ECMWF integrated forecast system during the time period considered. For long-term studies, reanalysis data that are generated with a "frozen" model and data assimilation system would be preferable but time consistency is not crucial for the rather short period of this study. We used the operational data because of the higher quality compared to the reanalysis datasets from ECMWF (higher spectral resolution and, for the later years, an improved data assimilation).

In this study we trace $E - P$ both forward from the earth's ocean basins and backward from river catchments. To distinguish between the different ocean basins, we used digital data with 1° resolution from the *World Ocean Atlas* (Conkright et al. 2002). The ocean basins are shown in Fig. 1 and their names are listed in Table 1. We investigated 39 river basins, for which gridded geographical data with 0.5° resolution were obtained from the Global Runoff Data Center (Vörösmarty et al. 2000; Fekete et al. 2000). These river systems are shown in Fig. 2 and their names are listed in Table 2. The basins were selected subjectively, but they include the world's largest rivers and at least one river from every continent.

3. Validation of $E - P$ estimates for the river basins

In Part I we validated $E - P$ fields calculated with the Lagrangian method by comparing them with $E - P$ fields from an established Eulerian diagnostic (Trenberth 1997) and with model forecasts of E and P. Here we provide additional validation. For large scales and long time periods, water mass conservation dictates that over land $E - P$ must be negative and balanced by the runoff into the ocean. For a river basin, in particular, the area-integrated $E - P$ must equal the streamflow into the ocean (ignoring groundwater discharge)

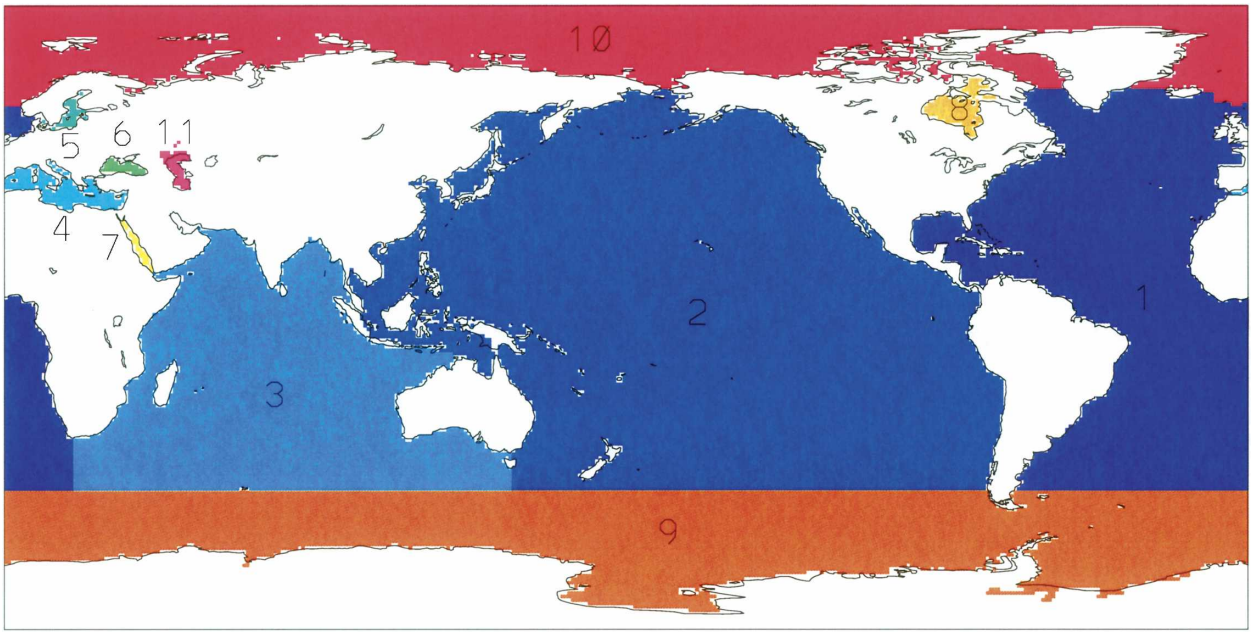

FIG. 1. Map of the ocean basins investigated. Basins are numbered as in Table 1; the colors are arbitrary.

for time periods long enough that changes in atmospheric and terrestrial water storage become insignificant (Seneviratne et al. 2004), which is typically one to a few years (Gutowski et al. 1997). River-mouth streamflow data can, therefore, be used to validate $E - P$ estimates.

Unfortunately, stations gauging the streamflow are normally not located directly at the river mouth but further upstream. We therefore use data from Dai and Trenberth (2002) who have combined streamflow data from the world's 200 largest rivers' farthest downstream stations with a river transport model to estimate the long-term mean river-mouth streamflows. There are several caveats in comparing our $E - P$ estimates with the Dai and Trenberth (2002) climatology. First, the 4-yr period studied here may be different from the climatology. The standard deviation of annual streamflow is some 10%–30% of the mean flow for the largest river basins, but it can be much larger for smaller basins (Dai and Trenberth 2002). Second, the streamflow data used by Dai and Trenberth (2002) also contain uncertainties of typically a few percent (Seneviratne et al. 2004). Third, differences between the streamflow at the farthest downstream station and the estimated streamflow at the river mouth can be substantial, in some cases more than a factor of 2. In these cases, the values at the river mouth are sensitive to errors in the river transport model used by Dai and Trenberth (2002). Fourth, smaller river basins are not well resolved by the 1° resolution of the ECMWF data and area integration of $E - P$ can be quite erroneous. This is particularly important in mountainous regions where a substantial fraction of the precipitation can occur close to the division between watersheds. Fifth, changes in terrestrial water storage over the 4-yr period would also introduce an error. This is especially relevant at high latitudes, where changes in snowpack can be significant, and in arid or semiarid regions, where substantial changes in

TABLE 1. Net freshwater flux $E - P$ expressed as both basin total annual mass flux (km^3 yr^{-1}) and mass flux per area (mm yr^{-1}) over the world's ocean basins for the period Dec 1999 to Nov 2003. Basins are numbered (N) as in Fig. 1.

N	Ocean basin	km^3 yr^{-1}	mm yr^{-1}	N	Ocean basin	km^3 yr^{-1}	mm yr^{-1}
1	Atlantic Ocean	27 509	371	7	Red Sea	381	1317
2	Pacific Ocean	4581	29	8	Hudson Bay	−265	−320
3	Indian Ocean	18 979	323	9	Southern Ocean	−22 572	−493
4	Mediterranean Sea	1454	746	10	Arctic Ocean	−2439	−200
5	Baltic Sea	−39	−175	11	Caspian Sea	137	273
6	Black Sea	74	233				

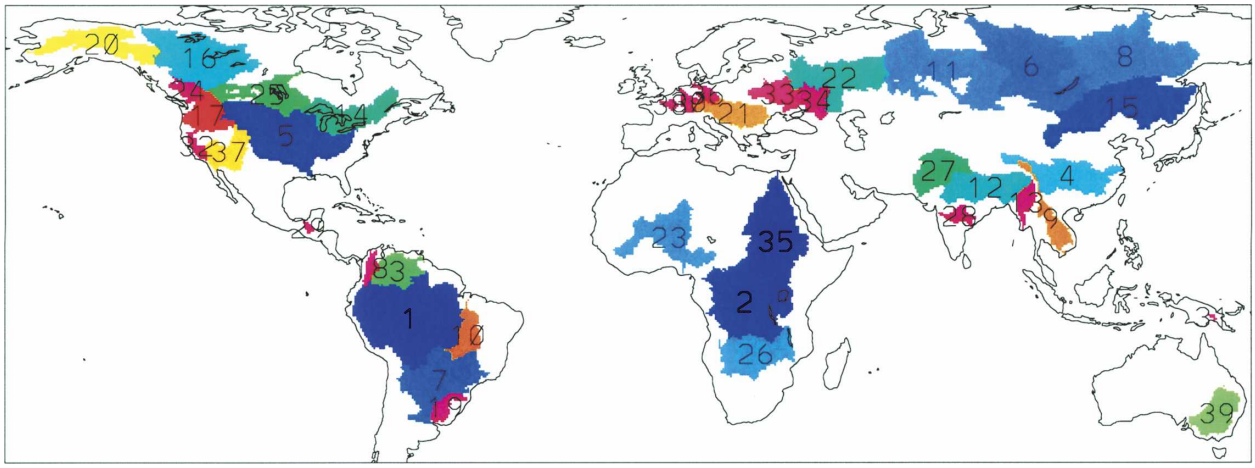

FIG. 2. Map of the river basins investigated. Basins are numbered as in Table 2; the colors are arbitrary.

subsurface water storage can occur. We estimate, subjectively, that all errors together add up to about 25% for the largest river basins and about 50% for smaller basins. Larger differences likely indicate errors in the $E - P$ fields.

Figure 3 shows a scatterplot of 4-yr-average river-basin-integrated $P - E$ values versus the climatological river-mouth streamflow data of Dai and Trenberth (2002). There is a relatively good agreement between the two datasets, especially for many of the largest river basins. A regression analysis between the 39 values of the two datasets yields an explained variance of more than 87% with a slope of 0.61 and an intercept of 61 $km^3\ yr^{-1}$. For some of the river basins, however, there is a significant imbalance between $P - E$ and the river-mouth streamflow (Table 2). For the world's largest river, the Amazon, for instance, $P - E$ underestimates the river-mouth streamflow by 40%, a fact that has been noted in previous studies (e.g., Dai and Trenberth 2002). For the next three largest basins, however, the agreement is better than 13%, with $P - E$ slightly overestimating the streamflow. For the fifth largest river, the Mississippi, the streamflow is underestimated by 16%. This imbalance is comparable to or smaller than

TABLE 2. Comparison of the freshwater discharge ($km^3\ yr^{-1}$) from 39 selected river catchments estimated using the Lagrangian diagnostic ($P - E$) for the period Dec 1999–Nov 2003, and climatological river-mouth flows estimated by Dai and Trenberth (2002) (DT02). Catchments are numbered (N) as in Fig. 2.

N	River	DT02	$P - E$	N	River	DT02	$P - E$
1	Amazon	6642	3796	21	Danube	202	142
2	Zaire/Congo	1308	1473	22	Volga	200	261
3	Orinoco	1129	1229	23	Niger	193	−360
4	Chang Jiang	944	1041	24	Fraser	144	112
5	Mississippi	610	514	25	Nelson	126	137
6	Yenisey	599	527	26	Zambezi	117	−239
7	Parana	568	287	27	Indus	104	−267
8	Lena	531	357	28	Godavari	97	−84
9	Mekong	525	368	29	Usumacinta	89	−7
10	Tocantins	511	153	30	Rhine	75	48
11	Ob	412	517	31	Purari	74	66
12	Ganges	404	881	32	Sacramento	69	−16
13	Irrawaddy	393	591	33	Dnepr	47	4
14	St. Lawrence	363	373	34	Don	45	21
15	Amur	354	102	35	Nile	40	172
16	Mackenzie	290	312	36	Elbe	27	7
17	Columbia	252	149	37	Colorado	12	50
18	Magdalena	231	241	38	Seine	11	28
19	Uruguay	228	446	39	Murray	9	−248
20	Yukon	212	211				

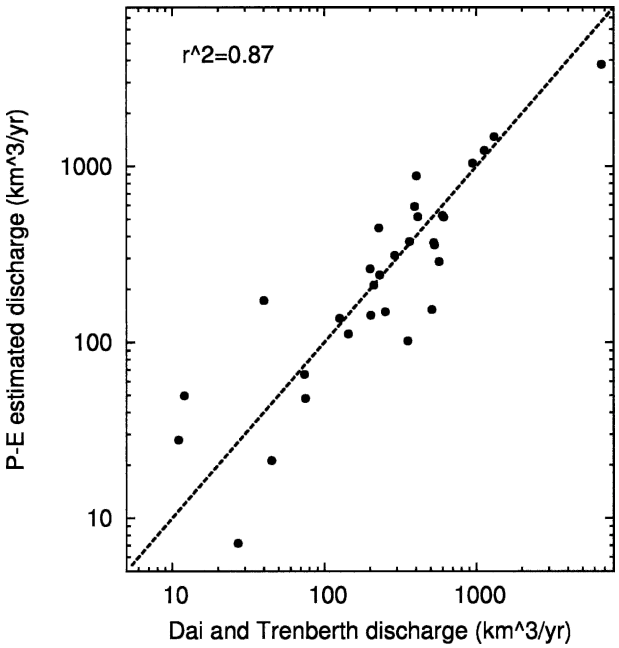

FIG. 3. Scatterplot of 4-yr-average river-basin-integrated annual $P - E$ obtained with the Lagrangian method vs the climatological annual river-mouth streamflow data taken from Dai and Trenberth (2002). Values are for the 39 river basins listed in Table 1. Eight river basins are not shown because of too small or negative $P - E$. The dashed line represents a 1:1 relationship.

others published for the same river basin (Seneviratne et al. 2004) or its subbasins (Gutowski et al. 1997). Our $P - E$ estimates compare favorably also with previous estimates for the Mackenzie (Smirnov and Moore 2001; Serreze et al. 2003) and the Ob and Yenisey (Serreze et al. 2002). For the Lena basin a previous study reported better agreement (Serreze et al. 2002). Agreement is generally less good for smaller basins because the accuracy of moisture convergence calculations decreases with a basin's size (Rasmusson 1968). For seven river basins $P - E$ is negative, indicating that moisture diverges over these basins in the 4-yr average. Such severe discrepancies between $P - E$ and streamflow have also been reported in other studies (Liu and Stewart 2003) and may be due to fundamental problems in the ECMWF model's water cycle (Betts et al. 2003) or lack of resolution. A reviewer also suggested that groundwater withdrawal is a plausible reason for the Sacramento and Murray basins, but the negative $P - E$ values may also indicate that the 4-yr period was too short to assume no changes in the water storage for some of the basins.

Even though this comparison indicates significant problems with our $E - P$ estimates for some river basins, the results are within the error bounds of the streamflow data for many river basins and compare favorably with other studies (Gutowski et al. 1997; Smirnov and Moore 2001; Dai and Trenberth 2002; Serreze et al. 2002; Liu and Stewart 2003; Seneviratne et al. 2004). Therefore, and also based on the validation presented in Part I, we conclude that our $E - P$ tracking is based on a solid methodology of diagnosing $E - P$.

4. $E - P$ tracking—The technique and some examples

In this section, we will present two examples. We will track the moisture from the Mediterranean Sea forward to see in which regions water from originally Mediterranean air masses is lost. And we will track the air masses residing (and also only those precipitating) over the Mississippi basin back in time to see where the moisture originated.

To quantify the net exchange of moisture between river catchments and ocean basins (henceforth referred to collectively as basins), all the particles residing over a given target basin—together representing the entire mass of air over that basin—were identified every 3 h and tracked forward or backward for 10 days. The estimate $E - P$ during the first trajectory time step (when all the target particles reside over the target basin by definition) is exactly the basin-integrated net freshwater flux. Annual means of these values are reported in Tables 1 and 2 and were compared with the river discharges in the previous section.

Particles leaving their arrival/departure basin gain or lose moisture over other basins. Applying Eq. (2) (disregarding the first time step) along the trajectories of the target particles, therefore, yields $E - P$ for these basins under the condition that the particles travel to (for backward tracking) or arrive from (for forward tracking) the target basin. Note that, as the target particles disperse, the particles residing in an atmospheric column do not represent its entire atmospheric mass anymore, but only that part of the column fulfilling the criterion that it later (earlier) reaches the target basin. Conditional $E - P$ values, subsequently referred to as $(E - P)_c$, therefore, do not represent the surface net freshwater flux, but only the net freshwater flux into the air mass traveling to (arriving from) the target basin. Moisture can also come from evaporating rain droplets received from a precipitating overhead air mass that is not accounted for. Similarly, water can be lost without necessarily producing rain at the surface if droplets evaporate in drier unaccounted air lying underneath the tracked air mass. Also, mixing with other air masses may decrease or increase the tracked air mass' moisture content. Our method cannot distinguish these fluxes from surface fluxes.

Another weakness of the method is that the entire air mass lying over an ocean basin is tracked forward or backward in time, regardless of whether it had recent contact with the ocean surface or not. This also means that the moisture evaporated over the basin is not kept track of itself. Instead, it is only diagnosed where an air mass originally located over the source basin loses or gains moisture as it travels away from the source.

Trajectory accuracy is critical for our method as trajectory errors can lead to systematic $(E - P)_c$ errors. For instance, if a particle is tracked forward from an ocean basin in a relatively moist air mass but leaves that air mass over time because of trajectory errors, q decreases along its trajectory, leading to erroneous diagnosis of $(E - P)_c < 0$. Therefore, $(E - P)_c$ will be systematically too small (large) for the forward tracking from moist (dry) regions. We will come back to this issue in section 6.

Budgets for all target basins were calculated on a $1^\circ \times 1^\circ$ grid and were averaged over monthly periods. The $(E - P)_c$ values were binned into 10 daily "age" classes, according to the time backward or forward along the trajectories. That way, both where and when moisture was received or lost can be determined. We present the $(E - P)_c$ values either for a certain day (e.g., on the fifth day of the tracking) or integrated from the start of the tracking to a certain day (e.g., the sum of days 1–5). To distinguish these two forms, we use the nomenclature $(E - P)_c^n$ to show $(E - P)_c$ on day n, and $(E - P)_c^{n,i}$ to show $(E - P)_c$ integrated over days 1 to n (or -1 to n for backward tracking when n is negative).

While the 10-day period of tracking chosen here is somewhat arbitrary, it is about the average residence time of water vapor in the atmosphere (Numaguti 1999) and it is also a period over which the trajectories can be considered relatively accurate (Stohl 1998). Furthermore, toward the end of the 10-day period, the patterns in the $(E - P)_c$ fields tend to converge toward the patterns of the unconditional $(E - P)$ fields (see below), as the particles lose memory of their original position and humidity. From the gridded output, source–sink matrices between the 39 river and 11 ocean basins were constructed.

To illustrate the forward tracking, we take the case of the Mediterranean Sea, which is a strong net source of water vapor (see Table 1). Figure 4 shows the $(E - P)_c$ fields for winter on the first, third, and tenth day of transport, and averaged over all 10 days.[1] As air masses travel away from the Mediterranean, they lose moisture over the surrounding land areas, particularly over Europe (see Figs. 4a and 4b for days 1 and 3). Moisture loss is less pronounced over Africa and subtropical Asia, where moisture actually increases in some regions. Moisture also increases over the Red Sea, whereas it decreases over the Black Sea, as also seen in the 10-day average (Fig. 4d). The Black Sea is a basin with net evaporation in the unconditional $E - P$ fields (see Table 1), but air arriving from the Mediterranean actually loses moisture there. On day 10, particles have spread over much of the Northern Hemisphere and the $(E - P)_c^{10}$ patterns become more similar to the unconditional ones (see Fig. 1 in Part I) as the air loses memory of its Mediterranean origin.

Figure 5 shows time series of $(E - P)_c^i$ from forward calculations from the Mediterranean and integrated over certain basins. Mediterranean air loses about 69 km^3 per winter season of water above the Danube basin, most of it within the first 4 days of transport because of the proximity of the two basins. Mediterranean air loses even more water over the Volga and Ob basins but because of the longer distance, the moisture loss starts only after 2 and 3 days, respectively, and is still ongoing on day 10, particularly for the Ob. Mediterranean air also loses moisture over the Black Sea between days 1 and 4, but it gains significant amounts of moisture over the Red Sea, which globally is the ocean basin with the highest net evaporation, more than 1300 mm yr^{-1}.

As an example for the backward tracking, we take the Mississippi River (Fig. 6, showing annual mean conditions), because for this basin several studies of the moisture source regions are available for comparison (Dirmeyer and Brubaker 1999; Brubaker et al. 2001; Bosilovich et al. 2003). Most of the air still resides over the North American continent one day back in time (Fig. 6a), but some air also comes from the Pacific and the Gulf of Mexico. The value $(E - P)_c^{-1}$ is negative over western North America, where air must rise over the mountainous topography, and over the southeastern United States, where moist air arrives from the Gulf of Mexico (see later). The value for $(E - P)_c^{-1}$ is positive over much of central North America, including the Mississippi basin itself, indicating the importance of moisture recycling (Eltahir and Bras 1996) over the continent (this feature is more prominent in summer than in winter). The value $(E - P)_c^{-2}$ (Fig. 6b) is strongly negative over the Pacific and the North American west coast, indicating that in these regions precipitation typically occurs in air masses in transit to the Mississippi. On the other hand, $(E - P)_c^{-2}$ is strongly positive over the Atlantic and, especially, over the Gulf

[1] Note that here we average the daily $(E - P)_c$ fields instead of integrating them in order to be able to use the same color scale as for the daily fields.

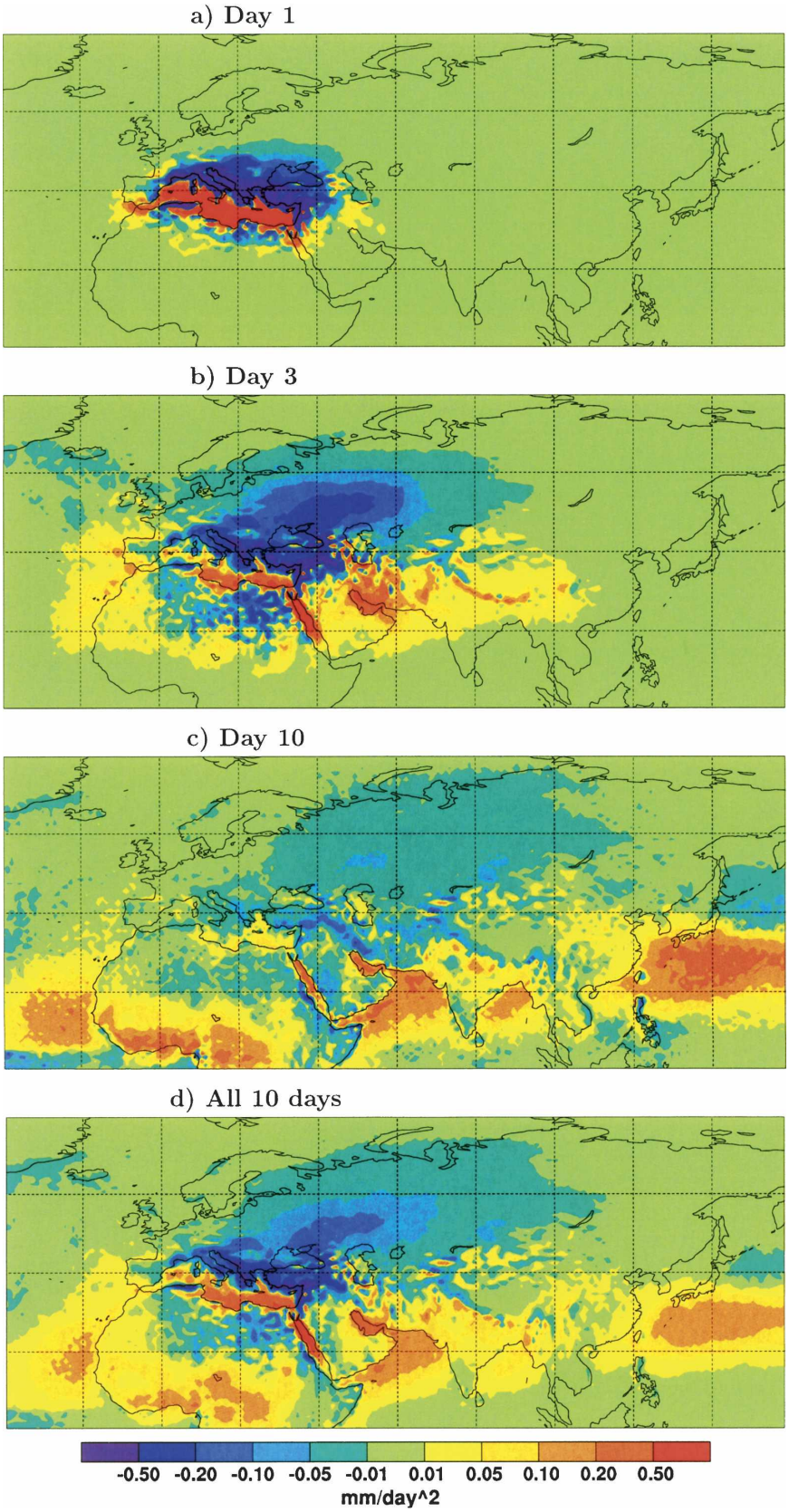
a) Day 1
b) Day 3
c) Day 10
d) All 10 days
-0.50 -0.20 -0.10 -0.05 -0.01 0.01 0.05 0.10 0.20 0.50
mm/day^2

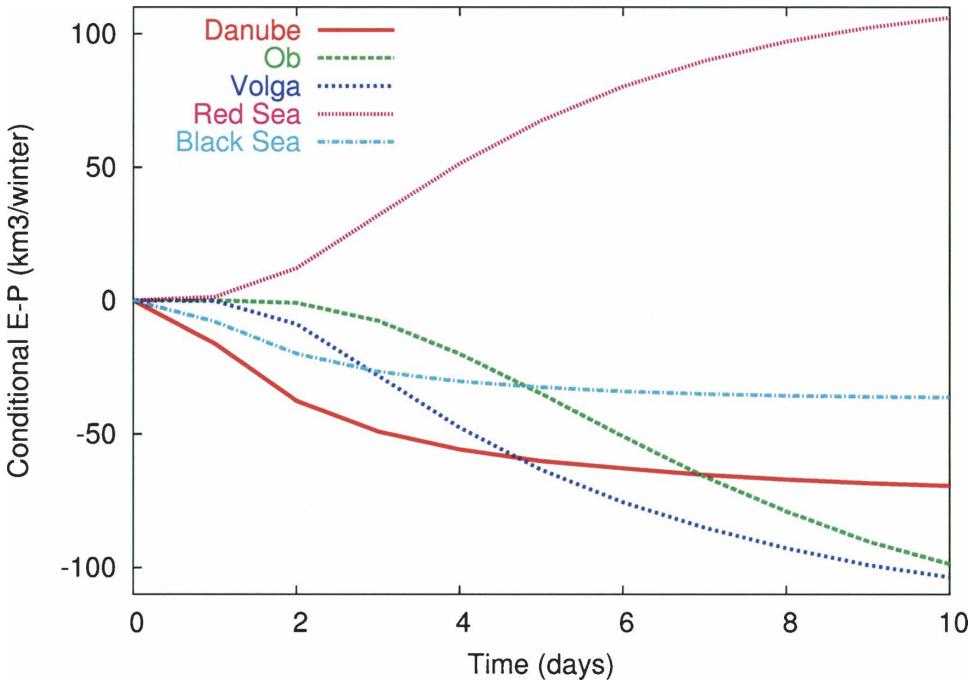

FIG. 5. Time series of $(E - P)_c^i$ calculated forward from the Mediterranean Sea and integrated over the Danube (red), Ob (green), and Volga (blue) catchments, and over the Red Sea (purple) and Black Sea (turquoise) basins, for winter.

of Mexico. Averaged over all 10 days of transport (Fig. 6c), relatively strong moisture uptake is diagnosed both over North America itself and the Gulf of Mexico, the Caribbean, and the warm waters close to the eastern seaboard of North America. In addition, the subtropical Pacific also appears as a net moisture source. However, as indicated by the negative $E - P$ values in Figs. 6a and 6b, much of the moisture may be lost west of the Rocky Mountain chain during the 2 days before the air actually reaches the Mississippi basin.

In the above analysis, all the air over the Mississippi basin was tracked back, regardless of whether it was raining over the basin or not at the time of arrival. We repeated the above analysis, but only for particles that lost moisture in a Mississippi basin grid cell where $E - P < -8$ mm per 3-h time step (Fig. 7). The annual mean $E - P$ over the Mississippi basin, diagnosed using only these particles, was -563 mm yr^{-1}, somewhat less than the actual observed precipitation of 780 mm yr^{-1} (Roads et al. 2003). A similar criterion was used already in our companion paper to identify particles producing precipitation during a flooding event. While the exact value of the $E - P$ threshold is certainly subjective, we tested the sensitivity by varying its value from 6 to 10 mm per 3-h time step. With the 8-mm threshold the annual average $P - E$ is below the observed precipitation over most basins, thus yielding a conservative identification of precipitating air masses. Furthermore, while the magnitudes vary, the patterns of the $(E - P)_c$ fields are very robust against changes of the $E - P$ threshold.

Tracing back the selected particles (Fig. 7) shows that few of them arrive from the Pacific. Actually, $(E - P)_c$ for the precipitating particles is close to zero over the entire Pacific, except over the Gulf of California and just west of Baja California. In contrast, $(E - P)_c$ is highly positive over both the North American continent (again pointing toward moisture recycling) and the Atlantic Ocean, particularly the Gulf of Mexico. The region of strongly negative $(E - P)_c^{-1}$ over the southeastern United States is caused by particles arriving from the Gulf of Mexico and traveling northwestward, pro-

←

FIG. 4. $(E - P)_c$ fields for the Mediterranean Sea for winter (Dec–Jan–Feb): (a) $(E - P)_c^1$ on day 1 of the forward tracking, (b) $(E - P)_c^3$ on day 3 forward, (c) $(E - P)_c^{10}$ on day 10 forward, and (d) $(E - P)_c^{10,i}$ (10 days)$^{-1}$, i.e., averaged over all 10 days of the forward tracking.

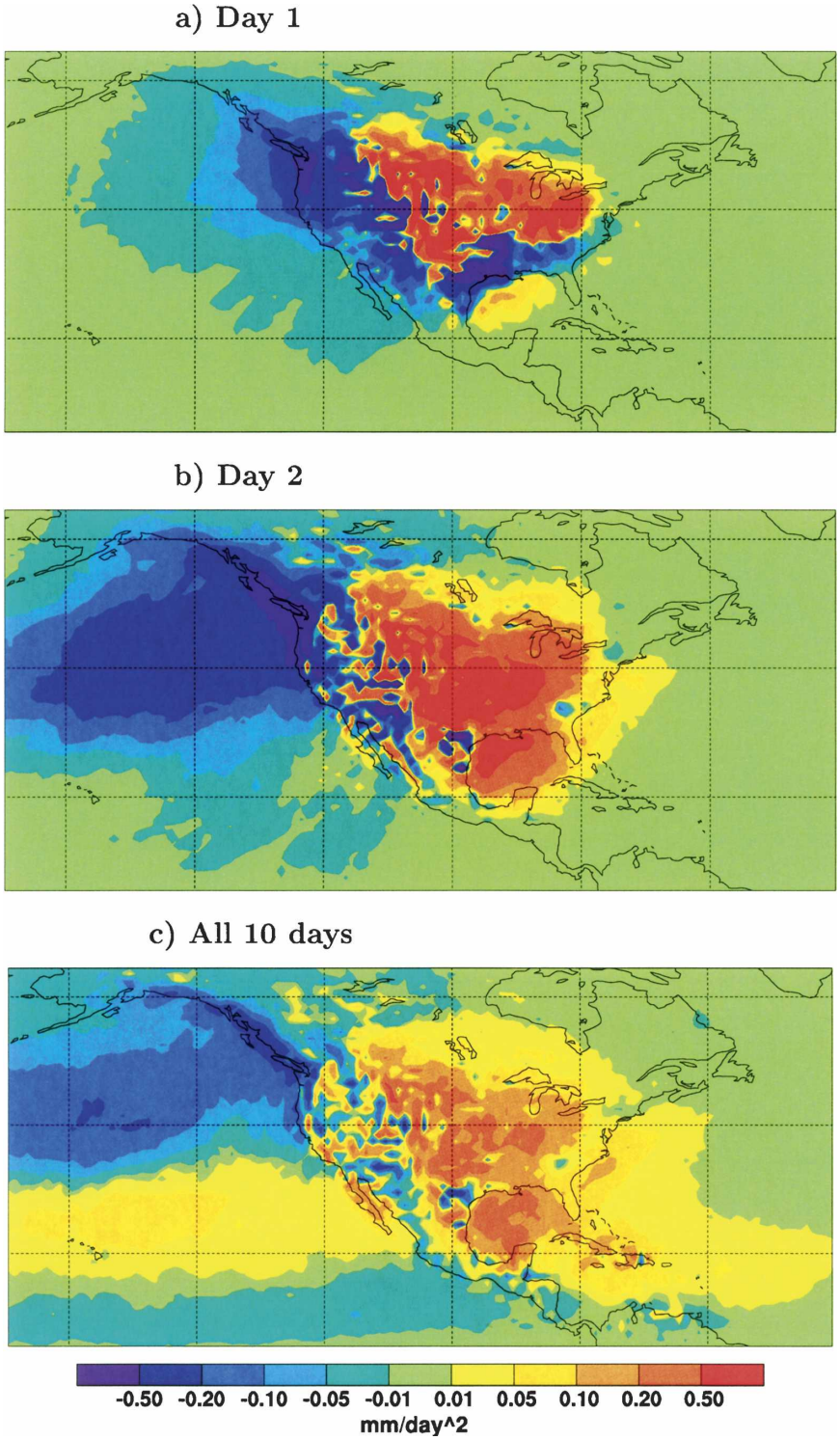

FIG. 6. Annually averaged $(E - P)_c$ fields for the Mississippi basin from the backward tracking: (a) $(E - P)_c^{-1}$, (b) $(E - P)_c^{-2}$, and (c) $(E - P)_c^{-10,i}$ (10 days)$^{-1}$, i.e., averaged over 10 days back.

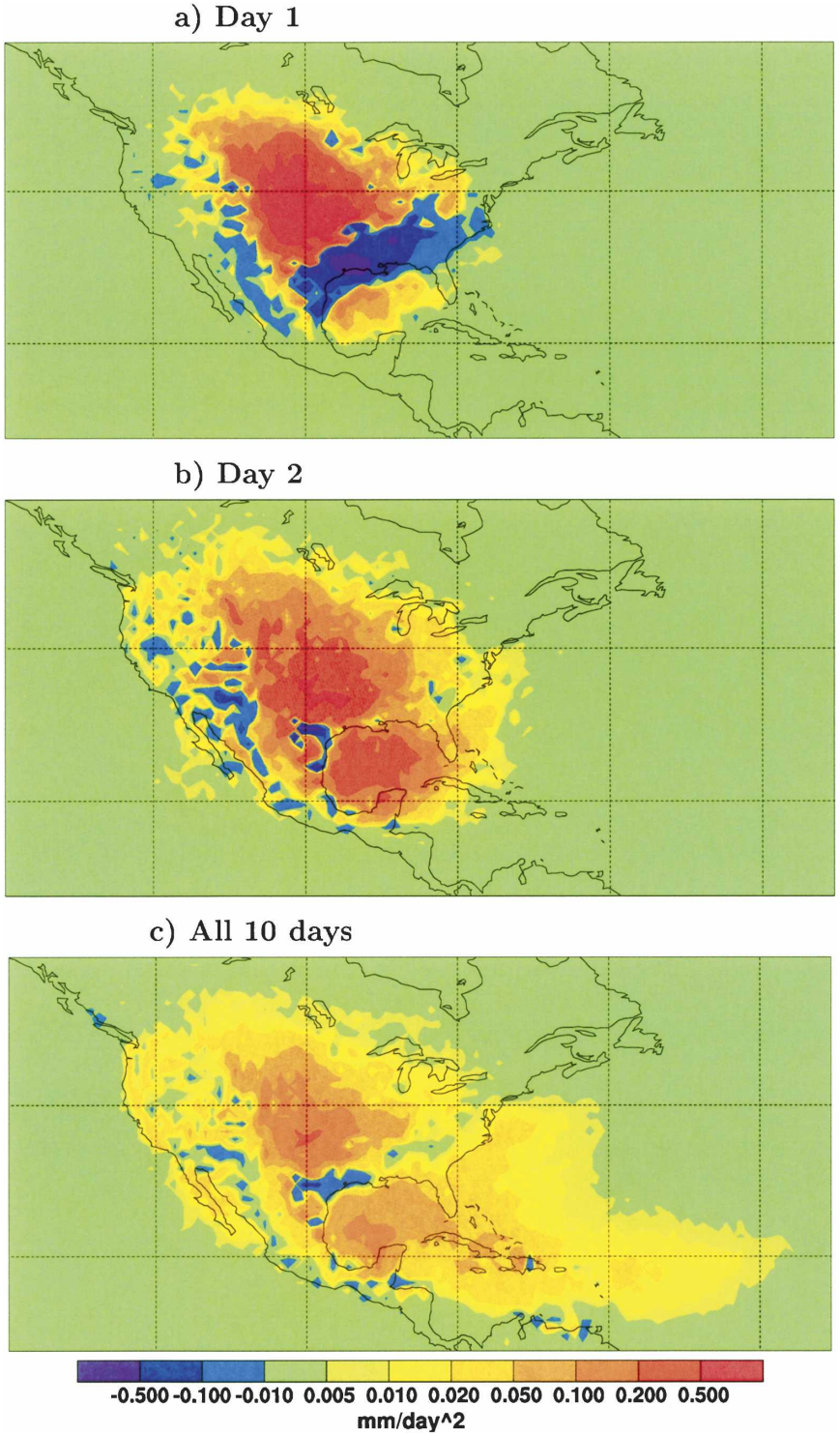

FIG. 7. Same as Fig. 6, but calculated only for precipitating particles with $dq(dt)^{-1} < 0$ g kg^{-1} (3 h)$^{-1}$ and arriving in a grid cell with $E - P < -8$ mm (3 h)$^{-1}$.

ducing precipitation already en route to the location from where they were traced back. In summary, our results indicate two major moisture source regions for precipitation falling over the Mississippi basin: recycling over the continent, and transport from the Atlantic Ocean, particularly from the Gulf of Mexico.

How does this compare with other studies? The patterns of the evaporative source regions for rain falling over the Mississippi basin from Dirmeyer and Brubaker (1999) and Brubaker et al. (2001) are generally very similar to our 10-day-average plot (Fig. 7c). Also, the magnitude of the evaporative strength is comparable. They find (Fig. 2 in Brubaker et al. 2001) about 32–64 mm per spring or summer season for the Gulf of Mexico, whereas our corresponding $(E - P)_c^{-10,i}$ (10 days)$^{-1}$ value from Fig. 7c is 0.05–0.1 mm (day)$^{-2}$ in the same region (this also holds for spring and summer only). Integrating over the 10-day period and multiplying by 90 days (roughly the length of a spring or summer season) gives 45–90 mm, which is only slightly higher than the values of Dirmeyer and Brubaker (1999) and Brubaker et al. (2001). The values over the continent are in good agreement, too. However, our maximum stretches farther east into the Atlantic Ocean and not as far south.

We cannot confirm that the Pacific Ocean is also a small but significant source of the Mississippi precipitation, as found by Dirmeyer and Brubaker (1999) and Brubaker et al. (2001). Their 16-mm isoline [which would correspond to 0.018 mm (day)$^{-2}$ in Fig. 7c] extends at least 500 km into the Pacific Ocean, where our $(E - P)_c^{-10,i}$ (10 days)$^{-1}$ value is almost an order of magnitude smaller. Actually it is hard to understand how the Pacific can be a major moisture source for precipitation over the Mississippi basin, as Pacific air has to cross the Rocky Mountains or the Sierra Madre to reach the Mississippi. While crossing these mountain chains, most of the moisture should be lost. This may have been less effective in the dataset used by Dirmeyer and Brubaker (1999) and Brubaker et al. (2001) because of its lower resolution and, thus, lower mountain crest height, leading to an overestimate of water vapor transport across the Rocky Mountains. Indeed, in a water vapor tracer study using a GCM Bosilovich and Schubert (2002) found that the North Pacific contributes only 2.2% of the summer precipitation in the southeastern United States. In a similar study, Bosilovich et al. (2003) found that the North Pacific contributes less than 15% to Texas precipitation in winter and close to 0% in summer. This agrees well with our results.

Looking now at when the moisture was taken up before the air precipitated over the Mississippi (Fig. 8), we see again the strong contrast between the Pacific and the Atlantic Ocean. While for the Atlantic $(E - P)_c^i$ is positive and increasing linearly backward in time over the entire 10 days, $(E - P)_c^i$ is negative and decreases with time over the Pacific. The Mississippi basin itself is clearly the most important moisture source up to about 4 days back, after which most of the air has left the basin and $(E - P)_c^i$ remains almost constant. It takes 8 days back for the Atlantic to become a larger moisture source for the Mississippi than evaporation in the Mississippi basin itself. Also, other North American land areas supply significant amounts of moisture for precipitation over the Mississippi. This emphasizes the important role of relatively rapid precipitation recycling over land.

5. Global source–sink relationships

In the same manner as described in the previous section, $(E - P)_c$ was tracked forward from all ocean basins and backward from the river basins. Land areas outside the 39 river basins were collectively classified as "Other land." In this section we describe the results from a global point of view and for annual mean conditions.

a. Forward tracking from the ocean basins

Table 3 lists, for every ocean basin, annual mean (i.e., integrated over the whole study period and divided by the number of years) $(E - P)_c^{2,i}$, $(E - P)_c^{5,i}$, and $(E - P)_c^{10,i}$ integrated over receptor basins as obtained from the forward tracking. For every source ocean basin, the table contains entries for the four river and four ocean receptor basins with the largest absolute $(E - P)_c^{10,i}$ values as well as the total integral over all land and ocean surfaces, respectively. To make the values more comparable, they are expressed in units of the annual mean total precipitable water residing over the source basin. Generally, values tend to be smaller for the larger source basins where a large part of the tracked air remains over the basin itself during the period of tracking. For instance, within 10 days of transport, Pacific Ocean air masses lose 14 times their precipitable water content per year over land and gain as much as their original content over other oceans. In contrast, Red Sea air masses lose 72 times their precipitable water content over land and gain 58 times their precipitable water content over oceans. This shows the relatively larger role of transport for the smaller basins.

The air masses tracked forward from seven ocean basins (including the largest ones: Atlantic Ocean, Pacific Ocean, and Indian Ocean) have negative $(E - P)_c^{10,i}$ values over land; that is, they lose water over land as they travel away from their source. However, for air

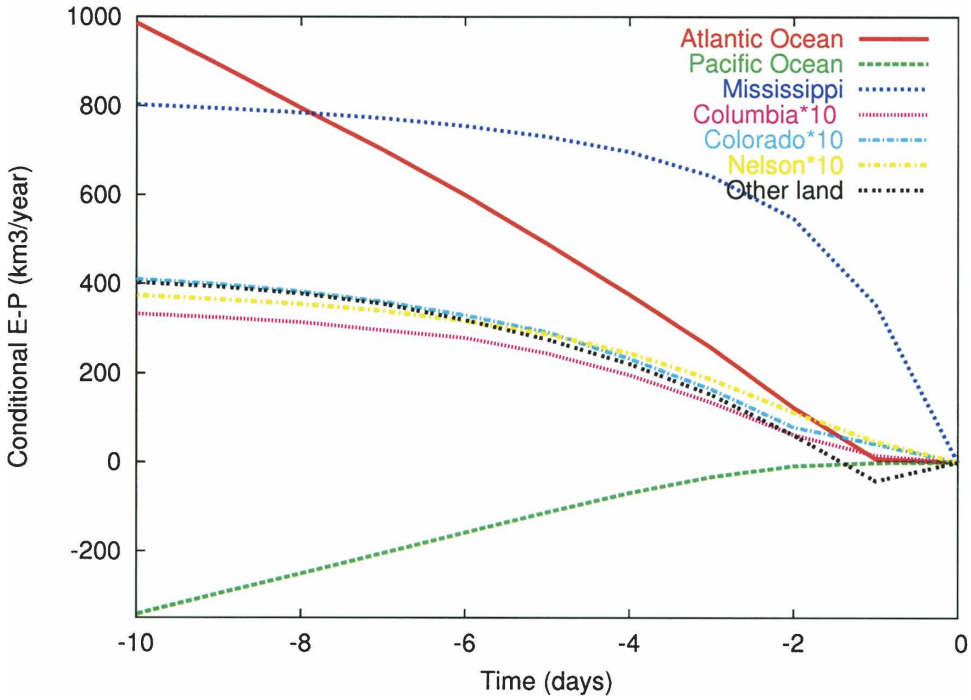

FIG. 8. Time series of $(E - P)_c^i$ calculated backward for particles precipitating over the Mississippi basin and integrated over the Atlantic Ocean (red) and the Pacific Ocean basins (green), and the Mississippi (blue), the Columbia (purple), the Colorado (turquoise), and the Nelson (yellow) river basins, and unclassified land areas (black). Values for the Columbia, CO, and Nelson basins are multiplied by 10.

masses tracked from four basins $(E - P)_c^{10,i}$ is positive over land. Three of these basins (Baltic Sea, Hudson Bay, and Arctic Ocean) are located at high latitudes and are indeed net moisture sinks (see Table 1). The fourth, the Mediterranean Sea, however, is a strong net source of water vapor (see Table 1) and one would expect air masses leaving the Mediterranean to provide moisture to the surrounding landmasses. This was indeed the case in the example for winter shown in the previous section (see Figs. 4 and 5), and, in fact, $(E - P)_c^{10,i}$ is negative over all Eurasian river basins north of the Mediterranean (Danube, Volga, Ob, Yenisey, Dnepr, Don, Lena, Rhine, Elbe, Seine) even in the annual mean. But Mediterranean air masses have strongly positive $(E - P)_c^{10,i}$ values over river basins to the south (Niger, Nile, Indus), especially in summer. The reason for this is the prevalence of anticyclonic conditions over the Mediterranean in summer, which suppress convection and prevent air masses aloft from having contact with the sea surface. When traveling southward, these air masses descend isentropically and arrive at the ground very dry, leading to moisture uptake. In the annual mean, Mediterranean air masses are, therefore, a net sink of moisture for the river basins in Africa and on the Indian subcontinent.

Figure 9 shows the annual mean $(E - P)_c^{10,i}$ fields for the earth's three major ocean basins: the Atlantic, Pacific, and Indian Oceans. Values are highest over the source basins, indicating that a large fraction of the tracked air masses typically remains over the respective source basin for part of (or even the entire) tracking time. The $(E - P)_c^{10,i}$ distributions over the source basins are qualitatively similar to the unconditional $E - P$ fields (see Fig. 1 in our companion paper), but there are also significant differences. For instance, in the North Atlantic storm track, negative $(E - P)_c^{10,i}$ values occur over much larger regions than in the corresponding unconditional $(E - P)$ fields, because no air masses are entering the basin from the North American continent over the 10-day tracking period. These air masses (and also those arriving from the Pacific; see below) are relatively dry and normally lead to evaporation over the North Atlantic. Without them being accounted for, precipitation dominates over evaporation over a much larger area of the North Atlantic than in the unconditional case. In the following, we concentrate on the $(E - P)_c^{10,i}$ patterns outside the respective source basins, thus focusing on moisture transport to other basins.

Air masses tracked from all three ocean basins are a significant source of moisture for the Arctic and South-

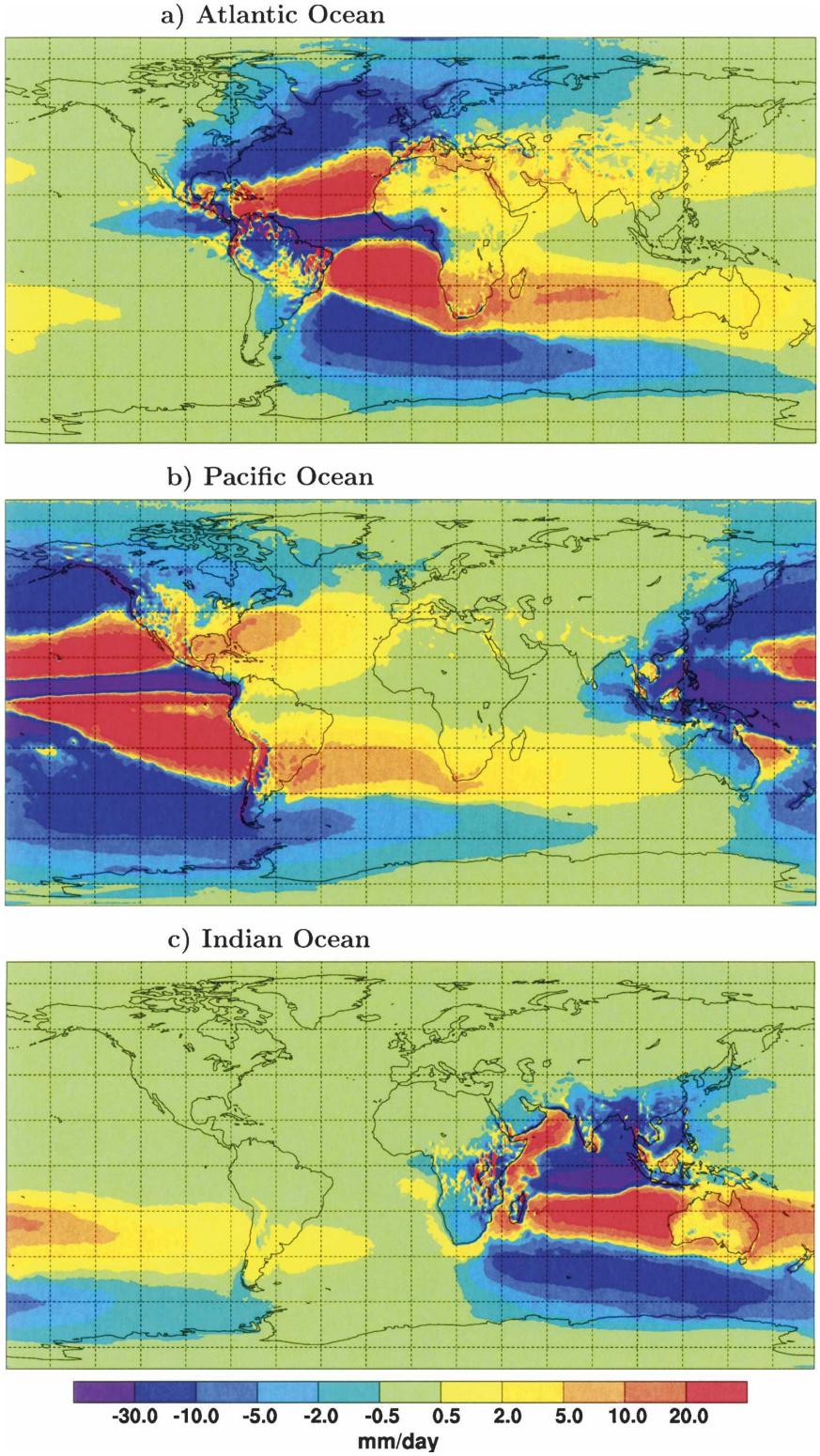

FIG. 9. Annual mean $(E - P)_c^{10,i}$ fields from forward tracking for (a) the Atlantic Ocean, (b) the Pacific Ocean, and (c) the Indian Ocean.

ern Oceans (Fig. 9). However, because of missing land barriers and its lower-latitude location, moisture transport into the Southern Ocean is much more effective than moisture transport into the Arctic Ocean. Air masses from the Atlantic, Pacific, and Indian Oceans supply 20, 15, and 33 times their average moisture content per year to the Southern Ocean, but only 3, 1, and 0 units, respectively, to the Arctic Ocean (all counted over the 10-day period of tracking; see Table 3). Thus, even considering the smaller size of the Arctic Ocean, much less freshening of the surface waters is produced there than in the Southern Ocean. In fact, over the 10 days of tracking, Atlantic, Pacific, and Indian Ocean air masses together lose 10^4 km^3 yr^{-1} of water over the Arctic Ocean, nearly 3 times the river discharge into the Arctic Ocean (Dai and Trenberth 2002). While a large part of this may eventually evaporate in underlying Arctic air masses instead of actually reaching the ocean surface and these values are biased high because of trajectory errors, the much higher values over the

TABLE 3. Annual mean $(E - P)_c^{2,i}$, $(E - P)_c^{5,i}$, and $(E - P)_c^{10,i}$ (values are listed in three subcolumns of every receptor basin's column) integrated over receptor basins and obtained from calculations forward from source ocean basins. Values are shown for the four river and ocean receptor basins with the largest absolute $(E - P)_c^{10,i}$ values as well as the total integral over all land and ocean surfaces, respectively. Values are expressed in units of the source basin's annual mean mass of precipitable water.

Source basin	Amazon			Mississippi			Orinoco			Zambezi			Total land		
Atlantic Ocean	0	−1	−6	0	−1	−3	0	−1	−3	0	1	2	−4	−10	−18
	Indian Ocean			Southern Ocean			Arctic Ocean			Mediterranean			Total ocean		
Atlantic Ocean	0	5	27	−4	−12	−20	−1	−2	−3	0	1	2	−4	−10	6
	Parana			Amazon			Mackenzie			Chang Jiang			Total land		
Pacific Ocean	0	1	2	0	0	1	0	0	−1	0	0	−1	−3	−8	−14
	Southern Ocean			Atlantic Ocean			Indian Ocean			Arctic Ocean			Total ocean		
Pacific Ocean	−2	−8	−15	0	2	13	0	0	2	0	0	−1	−3	−7	−1
	Ganges			Irrawaddy			Mekong			Chang Jiang			Total land		
Indian Ocean	0	−1	−3	0	−1	−2	0	−1	−1	0	0	−1	−2	−6	−21
	Pacific Ocean			Southern Ocean			Atlantic Ocean			Red Sea			Total ocean		
Indian Ocean	0	6	35	−7	−20	−33	0	0	2	0	0	0	−7	−13	5
	Niger			Danube			Volga			Indus			Total land		
Mediterranean Sea	0	2	13	−3	−7	−9	−1	−4	−8	0	5	8	−11	−12	12
	Pacific Ocean			Indian Ocean			Atlantic Ocean			Red Sea			Total ocean		
Mediterranean Sea	0	2	44	0	3	21	0	3	13	1	6	10	0	8	77
	Ob			Amur			Dnepr			Yenisey			Total land		
Baltic Sea	−1	−4	−11	0	2	7	4	6	7	0	−2	−7	−6	14	16
	Pacific Ocean			Arctic Ocean			Mediterranean			Atlantic Ocean			Total ocean		
Baltic Sea	0	4	73	−6	−29	−49	2	14	27	2	9	24	−1	8	98
	Volga			Ob			Don			Yenisey			Totalland		
Black Sea	−8	−20	−25	−2	−13	−23	−6	−9	−11	0	−3	−9	−23	−63	−87
	Pacific Ocean			Mediterranean			Indian Ocean			Arctic Ocean			Total ocean		
Black Sea	0	7	79	13	30	37	0	3	15	0	−2	−7	13	40	132
	Nile			Ganges			Godavari			Zaire/Congo			Total land		
Red Sea	−8	−22	−31	0	3	3	0	1	3	0	1	2	−36	−73	−72
	Indian Ocean			Pacific Ocean			Atlantic Ocean			Caspian Sea			Total ocean		
Red Sea	−1	8	46	0	1	18	0	0	−5	0	−1	−2	−1	9	58
	St. Lawrence			Mississippi			Nelson			Mackenzie			Total land		
Hudson Bay	13	33	37	1	14	21	2	6	7	0	−1	−2	30	96	91
	Atlantic Ocean			Arctic Ocean			Mediterranean			Pacific Ocean			Total ocean		
Hudson Bay	29	280	440	−3	−9	−32	0	2	13	0	0	13	26	273	436
	Parana			Uruguay			Murray			Amazon			Total land		
Southern Ocean	0	1	4	0	1	1	0	1	1	0	0	0	−9	−12	−32
	Indian Ocean			Pacific Ocean			Atlantic Ocean			Red Sea			Total ocean		
Southern Ocean	26	135	273	24	134	271	15	87	183	0	0	0	66	356	727
	Ob			Lena			Volga			Amur			Total land		
Arctic Ocean	1	8	16	0	4	10	0	4	9	0	2	9	0	74	169
	Atlantic Ocean			Pacific Ocean			Mediterranean			Caspian Sea			Total ocean		
Arctic Ocean	8	46	144	2	27	129	0	4	14	0	1	4	10	81	301
	Ob			Volga			Yenisey			Indus			Total land		
Caspian Sea	−7	−27	−40	−7	−16	−19	−1	−8	−17	2	9	11	−15	−63	−109
	Pacific Ocean			Indian Ocean			Arctic Ocean			Mediterranean			Total ocean		
Caspian Sea	0	18	110	0	7	19	0	−3	−8	0	2	6	0	25	131

Southern Ocean indicate the great potential of atmospheric water vapor transport to high latitudes if there is no topography. In the current climate the densest ocean deep waters worldwide are formed in the Northern Hemisphere (Webster 1994), but would this still be the case if atmospheric water vapor transport into the Arctic Ocean were as effective as into the Southern Ocean?

Another big question in the study of the thermohaline circulation is why deep water formation occurs in the North Atlantic but not in the North Pacific (Weaver et al. 1999; Emile-Geay et al. 2003). Table 3 shows that Atlantic air masses are neither a source nor a sink of moisture for the Pacific over the 10-day time scale considered. In contrast, Pacific air masses trigger very strong evaporation over the Atlantic where they take up an additional 13 times their average moisture content per year. This asymmetry occurs in both hemispheres, but it is especially pronounced in the Northern Hemisphere (Fig. 9). There, strong moisture uptake into originally North Pacific air masses occurs over the North Atlantic up to latitudes of about 50°N, and even farther north there is little net moisture loss from North Pacific air masses (Fig. 9b). Thus, it appears that strong evaporation events (which increase the sea surface salinity) are triggered over much of the North Atlantic when Pacific air masses are transported over it but not vice versa. This feature is almost exclusively the result of the wintertime circulation and virtually not present in summer. The reason for this is that moisture is efficiently extracted from Pacific air masses over North America's topography. Especially in winter, little of the moisture lost is replaced by evapotranspiration over land and the originally North Pacific air masses arrive relatively dry over the North Atlantic, where they lead to strong evaporation. Instead, the moisture for precipitation over the high-latitude North Atlantic comes mostly from the lower latitudes of the North Atlantic itself (cf. Figs. 9a and 9b). Such an evaporation–precipitation cycle, however, has little net effect on the sea surface salinity given that surface ocean currents are also running northward in the subtropical and midlatitude North Atlantic. Furthermore, freshening of the North Pacific—but not of the North Atlantic—is produced by net precipitation in air masses coming from the Indian Ocean (Fig. 9c). In the Southern Hemisphere, in contrast, Indian Ocean air masses trigger strong net evaporation over much of the South Pacific.

Air masses originating from the high-latitude oceans (Hudson Bay, Arctic Ocean, and Southern Ocean) are extremely strong sinks of moisture when they are transported toward lower latitudes [Fig. 10 shows $(E - P)_c^{10,i}$ fields for the Arctic and Southern Ocean air masses]. Southern Ocean air masses, for instance, take up an additional 356 (727) times their average moisture content per year through net evaporation over the Indian, Pacific, and Atlantic Oceans within 5 (10) days (Table 3). Arctic Ocean air masses take up an additional 144 units over the Atlantic and 129 units over the Pacific within 10 days (note, again, the stronger uptake over the Atlantic despite its smaller area). For the Arctic Ocean air masses, net moisture uptake occurs not only over the Atlantic and Pacific but also over most of the Northern Hemisphere landmasses, except where topographic lifting can extract moisture from these cold air masses (mainly over Greenland and along the coast of Norway). Southern Ocean air masses lose moisture over the southern tip of South America and, particularly, along the Antarctic coastline.

This paper cannot go into regional details, but two features are noteworthy. While South Africa is surrounded by the Atlantic and Indian Oceans and is also close to the Southern Ocean, the only air masses causing net precipitation there are those from the Indian Ocean, a finding that agrees well with a regional study (D'Abreton and Tyson 1996). Over Australia, there is a strong contrast between Indian Ocean air masses, which cause net evaporation, and Pacific air masses, which produce net precipitation. The strong Pacific moisture source is in fact consistent with the moisture transport patterns during the Australian monsoon season (Godfred-Spenning and Reason 2002; Hung and Yanai 2004).

b. Backward tracking from the river basins

Table 4 presents the annual mean results for particles precipitating over the 39 river basins. The $(E - P)_c^i$ values are reported as percentages of the precipitation diagnosed over the target basin. For 15 of the 39 river basins total $(E - P)_c^{-2,i}$ values are negative, indicating that precipitation frequently starts before the particles moved into the target basin or fulfilled the target criteria. Seven basins also show negative $(E - P)_c^{-5,i}$ values but all $(E - P)_c^{-10,i}$ values are positive, indicating net moisture uptake prior to the precipitation event. For 28 basins, including all the large ones, $(E - P)_c^{-10,i}$ values exceed 100%; that is, more moisture is taken up during the 10 days before a precipitation event than is lost during it. Most of the values are moderately above 100%, indicating that the typical time scale of an evaporation/precipitation cycle is of the order of 10 days, without any clear systematic differences between tropical and extratropical basins.

It is relatively common (nine cases) that the target basin itself is the largest source of the precipitating water, indicating the global significance of precipitation

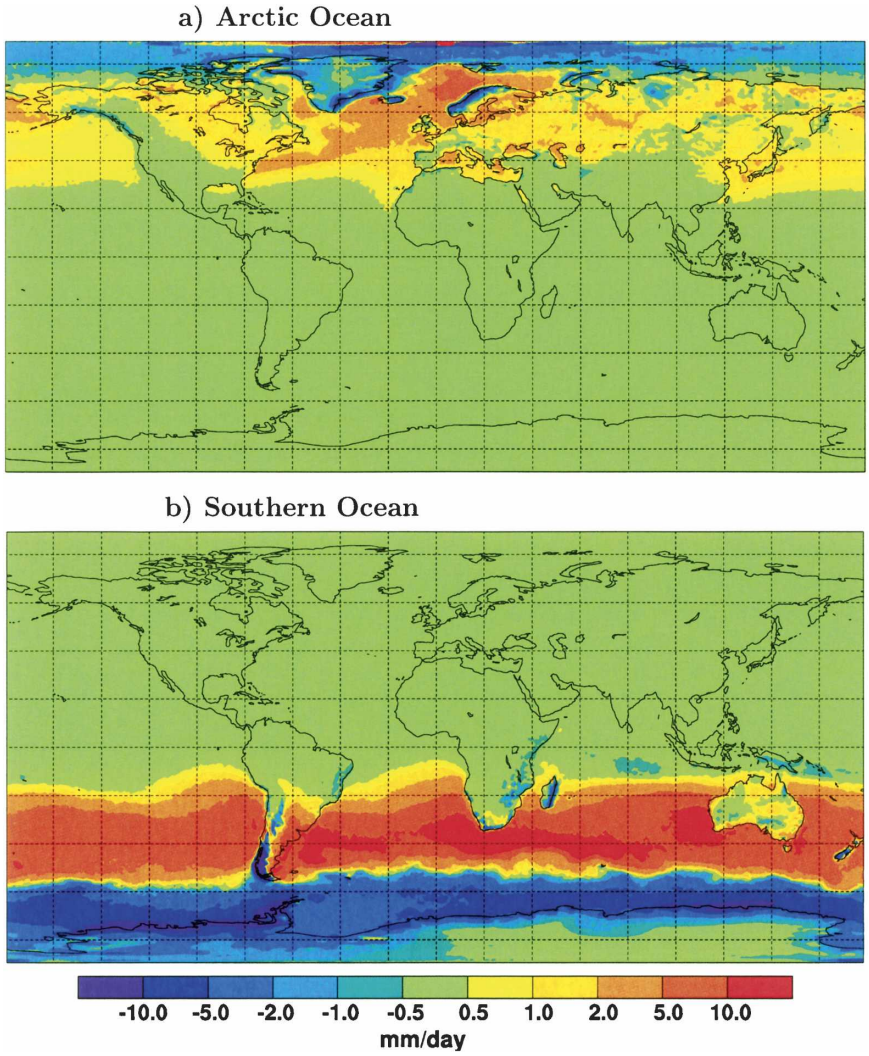

FIG. 10. Annual mean $(E - P)_c^{10,i}$ fields from forward tracking for (a) the Arctic Ocean and (b) the Southern Ocean.

recycling within the same catchment. If the concept of precipitation recycling is extended to also include moisture transport from other land surfaces, recycling becomes even more important. In 18 cases, the largest water vapor source over 10 days is not an ocean basin, and also in 18 cases less than 50% of the water comes from the oceans. This is particularly the case for the rivers in northern Eurasia (Volga, Dnepr, Don, Ob, Yenisey, and Lena) that are remote from ocean surfaces (except for the Arctic Ocean, which is a net moisture sink) and for which generally the basin itself, the basin to the east, and "other land" are the largest moisture sources. This is consistent with both westerly moisture fluxes and decreasing precipitation amounts from west to east over the Ob, Yenisey, and Lena basins during summer (Fukutomi et al. 2003). It is also consistent with the moisture flux convergence having a summer minimum despite the summer peak in precipitation, which has been explained with strong local surface evaporation and convection (Serreze and Etringer 2003). Serreze et al. (2002) have estimated the annual peak local recycling ratios over the Ob, Yenisey, and Lena basins to be 25%, 28%, and 22%, respectively, in July. As there is no universal definition of the recycling ratio and its associated length scale (see Eltahir and Bras 1996; Trenberth 1999), we may define it here as the ratio between the $(E - P)_c^{-10,i}$ over the target basin itself and totally. From Table 4 we thus obtain corresponding annual mean values of 32%, 36%, and 26%. These values are somewhat higher than the recycling ratios of Serreze et al. (2002), but they show the same behavior, that is, strongest recycling over the Yenisey

TABLE 4. Annual mean $(E - P)_c^{-2,i}$, $(E - P)_c^{-5,i}$, and $(E - P)_c^{-10,i}$ (values are listed in three subcolumns of every source basin's column) integrated over source basins and obtained from backward calculations from the 39 target river basins for precipitating particles [i.e., $dq(dt)^{-1} < 0$ g kg^{-1} (3 h)$^{-1}$ and $E - P < -8$ mm (3 h)$^{-1}$]. Values are expressed in percent of the diagnosed target precipitation and are shown for the entire globe (last column), and for the five source basins with the largest absolute $(E - P)_c^{10,i}$ values.

Target basin	Atlantic Ocean			Orinoco			Other land			Amazon			Tocantins			Total
Amazon	0	24	125	0	3	5	−5	−3	3	−21	−10	−3	−1	1	3	−26	17	134
	Zaire/Congo			Indian Ocean			Other land			Nile			Atlantic Ocean			Total		
Zaire/Congo	−18	9	30	0	0	24	1	7	20	0	9	18	0	3	13	−17	29	109
	Atlantic Ocean			Orinoco			Amazon			Other land			Tocantins			Total		
Orinoco	0	21	113	−31	−23	−21	−3	5	14	−4	−8	−6	0	0	1	−38	−6	100
	Pacific Ocean			Indian Ocean			Other land			Ganges			Irrawaddy			Total		
Chang Jiang	2	16	34	0	1	30	−8	1	14	−4	−9	−10	−4	−8	−9	−35	−4	65
	Atlantic Ocean			Mississippi			Other land			Pacific Ocean			Colorado			Total		
Mississippi	7	27	55	30	41	45	3	15	22	0	−6	−19	0	2	2	42	83	110
	Other land			Yenisey			Ob			Lena			Amur			Total		
Yenisey	7	28	51	20	43	49	3	17	27	3	7	9	2	4	6	35	98	137
	Atlantic Ocean			Parana			Amazon			Other land			Pacific Ocean			Total		
Parana	1	6	40	9	23	30	5	14	21	−1	4	12	0	−3	−11	15	50	103
	Lena			Amur			Other land			Yenisey			Ob			Total		
Lena	8	24	32	7	23	31	0	10	27	1	17	27	−1	3	7	14	76	122
	Indian Ocean			Pacific Ocean			Mekong			Irrawaddy			Chang Jiang			Total		
Mekong	−1	22	92	−7	−1	17	−15	−13	−12	−4	−4	−3	0	1	2	−45	−5	97
	Atlantic Ocean			Other land			Tocantins			Pacific Ocean			Amazon			Total		
Tocantins	1	47	163	8	30	37	−19	−15	−14	0	0	−2	−1	1	2	−12	62	185
	Other land			Ob			Volga			Atlantic Ocean			Yenisey			Total		
Ob	19	55	76	17	36	45	0	6	12	0	−1	−9	2	6	8	39	105	139
	Indian Ocean			Other land			Indus			Ganges			Irrawaddy			Total		
Ganges	2	25	96	1	14	34	1	11	19	−18	−15	−14	−3	−5	−7	−17	31	128
	Indian Ocean			Irrawaddy			Ganges			Other land			Godavari			Total		
Irrawaddy	1	34	134	−27	−26	−26	−15	−15	−13	−17	−7	9	1	4	5	−59	−12	112
	Atlantic Ocean			Mississippi			Pacific Ocean			Other land			Nelson			Total		
St. Lawrence	4	31	62	6	38	48	0	−7	−23	−4	13	21	−1	3	5	−2	77	116
	Amur			Other land			Pacific Ocean			Yenisey			Lena			Total		
Amur	21	39	47	−2	17	36	−1	4	15	0	4	8	1	4	8	18	67	113
	Mackenzie			Pacific Ocean			Nelson			Mississippi			Columbia			Total		
Mackenzie	14	28	31	−10	−23	−20	10	17	20	3	7	8	2	7	8	22	47	51
	Columbia			Pacific Ocean			Other land			Sacramento			Fraser			Total		
Columbia	44	49	49	−24	−1	12	5	10	7	2	5	5	2	3	3	29	66	72
	Atlantic Ocean			Orinoco			Magdalena			Pacific Ocean			Amazon			Total		
Magdalena	1	5	64	−28	−36	−34	8	18	22	1	9	17	−3	−7	−3	−22	−11	68
	Atlantic Ocean			Amazon			Parana			Other land			Pacific Ocean			Total		
Uruguay	2	9	40	2	14	21	−9	10	18	0	5	16	0	−5	−12	−17	26	80
	Yukon			Other land			Arctic Ocean			Mackenzie			Lena			Total		
Yukon	18	22	25	−23	−20	−19	−1	−4	−8	0	1	4	0	0	1	−50	−36	1
	Other land			Danube			Mediterranean			Dnepr			Volga			Total		
Danube	8	35	50	33	40	42	2	9	14	1	3	4	0	2	4	45	92	123
	Other land			Volga			Caspian Sea			Ob			Atlantic Ocean			Total		
Volga	16	49	68	15	26	32	8	13	16	3	9	15	0	−3	−9	44	111	146
	Atlantic Ocean			Niger			Other land			Mediterranean			Nile			Total		
Niger	2	19	62	20	31	36	2	16	31	0	0	5	0	−4	−3	24	62	132
	Pacific Ocean			Fraser			Other land			Columbia			Nelson			Total		
Fraser	−51	−10	21	18	20	20	−13	−9	−15	6	9	9	0	1	2	−40	12	32
	Mississippi			Pacific Ocean			Nelson			Other land			Columbia			Total		
Nelson	46	71	75	−1	−12	−27	11	19	21	4	13	17	3	10	11	65	112	116
	Indian Ocean			Other land			Zambezi			Zaire/Congo			Atlantic Ocean			Total		
Zambezi	3	25	78	2	10	16	−1	8	12	−1	1	4	0	1	3	2	44	111
	Indus			Other land			Indian Ocean			Atlantic Ocean			Irrawaddy			Total		
Indus	66	93	101	17	38	54	3	12	30	0	0	−6	0	0	−1	87	143	178
	Indian Ocean			Other land			Indus			Godavari			Ganges			Total		
Godavari	6	49	127	−7	6	31	0	4	9	3	5	5	−1	1	3	1	63	171
	Atlantic Ocean			Usumacinta			Orinoco			Other land			Pacific Ocean			Total		
Usumacinta	5	45	108	12	13	13	0	−2	−4	−4	3	3	−2	−5	2	11	53	123

TABLE 4. *(Continued)*

Target basin	Other land			Atlantic Ocean			Rhine			Mediterranean			Pacific Ocean			Total		
Rhine	8	34	42	−12	4	36	17	19	20	1	7	10	0	0	−4	16	66	103
	Pacific Ocean			Other land			Purari			Murray			Southern Ocean			Total		
Purari	5	61	158	−60	−65	−62	−32	−32	−31	0	0	1	0	0	0	−87	−36	65
	Pacific Ocean			Sacramento			Other land			Columbia			Amur			Total		
Sacramento	−18	19	49	28	31	32	5	8	8	0	1	2	0	0	−1	15	58	86
	Other land			Volga			Don			Danube			Dnepr			Total		
Dnepr	13	43	63	3	11	16	10	14	15	4	12	14	8	12	14	42	105	141
	Other land			Volga			Caspian Sea			Don			Atlantic Ocean			Total		
Don	16	52	72	10	18	23	14	19	21	12	15	16	0	−5	−14	57	119	150
	Nile			Other land			Indian Ocean			Zaire/Congo			Mediterranean			Total		
Nile	10	29	39	5	20	39	0	2	24	2	8	18	1	2	6	17	63	132
	Other land			Atlantic Ocean			Danube			Elbe			Mediterranean			Total		
Elbe	0	31	42	−5	4	20	7	11	13	11	12	12	−1	7	11	15	73	111
	Colorado			Other land			Pacific Ocean			Sacramento			Atlantic Ocean			Total		
Colorado	43	50	52	10	20	28	1	4	−4	1	2	2	0	0	1	56	76	80
	Atlantic Ocean			Other land			Mediterranean			Pacific Ocean			Rhine			Total		
Seine	−24	15	65	9	31	42	2	6	8	0	0	−6	3	4	4	−8	56	115
	Pacific Ocean			Murray			Other land			Indian Ocean			Southern Ocean			Total		
Murray	11	65	110	15	22	25	−2	11	23	1	3	5	0	−1	−5	24	99	155

and weakest recycling over the Lena basin. In fact, our recycling ratios are upper estimates, as the moisture present in the target air mass 10 days back (which probably has little local contribution) is not accounted for. Figure 11a shows the $(E - P)_c^{-10,i}$ field for the Yenisey. It is quite patchy, but it is clear that $(E - P)_c^{-10,i}$ is mostly positive over land and maximizes over and to the southwest of the Yenisey basin. On the other hand, $(E - P)_c^{-10,i}$ is close to zero over most ocean surfaces, in agreement with Brubaker et al. (1993) and water tracer studies (Numaguti 1999; Koster et al. 1986) that found that >80% of the summer precipitation in this region originates from the land.

While we cannot discuss all of the 39 river basins here, we present the results for 4 more basins from different continents and with vastly different moisture transport characteristics. Figure 11b shows the $(E - P)_c^{-10,i}$ field for the Ganges River. The dominant feature is a very large region of net evaporation over the Arabian Sea that stretches deeply into the Southern Hemisphere. The structure clearly reflects the southeasterly trade winds in the Southern Hemisphere that turn into the southwesterly monsoon at the equator. The monsoon air masses are most effectively transported toward the Ganges basin via northwestern India, as farther south moisture is lost over the Ghats mountains. A second moisture source region is India itself and the ocean east of it, whereas $(E - P)_c^{-10,i}$ is negative over the Ganges basin itself (Table 4). Moisture recycling over the basin itself appears not to be an important contributor to the precipitation over the Ganges.

Monsoonal flows are also important for the Niger (Fig. 12a). About half of the $(E - P)_c^{-10,i}$ originates from the Atlantic Ocean and the other half originates from over land (including the Niger basin itself). Moisture from the Atlantic Ocean is provided from the Southern Hemisphere via the southeasterly trade winds, which turn into the southwesterly monsoon flow in the Northern Hemisphere in summer. This transport route is not unlike the trajectories shown for tropical plumes causing extreme precipitation in western Africa (KM) and confines the oceanic moisture source region to a relatively small area off the African coast. Notwithstanding the fact that Mediterranean air masses, on average, produce net evaporation over the Niger basin (see Table 3), they also provide 5% of the Niger precipitation.

The dominant moisture source for the Amazon River, providing 125% of the identified precipitation over 10 days back in time, is the Atlantic Ocean (Fig. 11c). Moisture for the Amazon precipitation originates in two lobes of high $(E - P)_c^{-10,i}$ values over the Atlantic Ocean, which are separated by slightly negative $(E - P)_c^{-10,i}$ values in the intertropical convergence zone. The fact that moisture originates from the subtropics of both hemispheres is certainly key to why the Amazon is the world's largest river. Over South America, the $(E - P)_c^{-10,i}$ field is complicated and must be interpreted with caution, as the Amazon is one of the basins with the poorest agreement between basin-integrated $E - P$ and river-mouth streamflow (see Table 2). It appears that the Orinoco and the Tocantins basins are significant additional sources of moisture (Table 4), whereas $(E - P)_c^{-10,i}$ integrated over the Amazon basin itself is negative. However, there is an

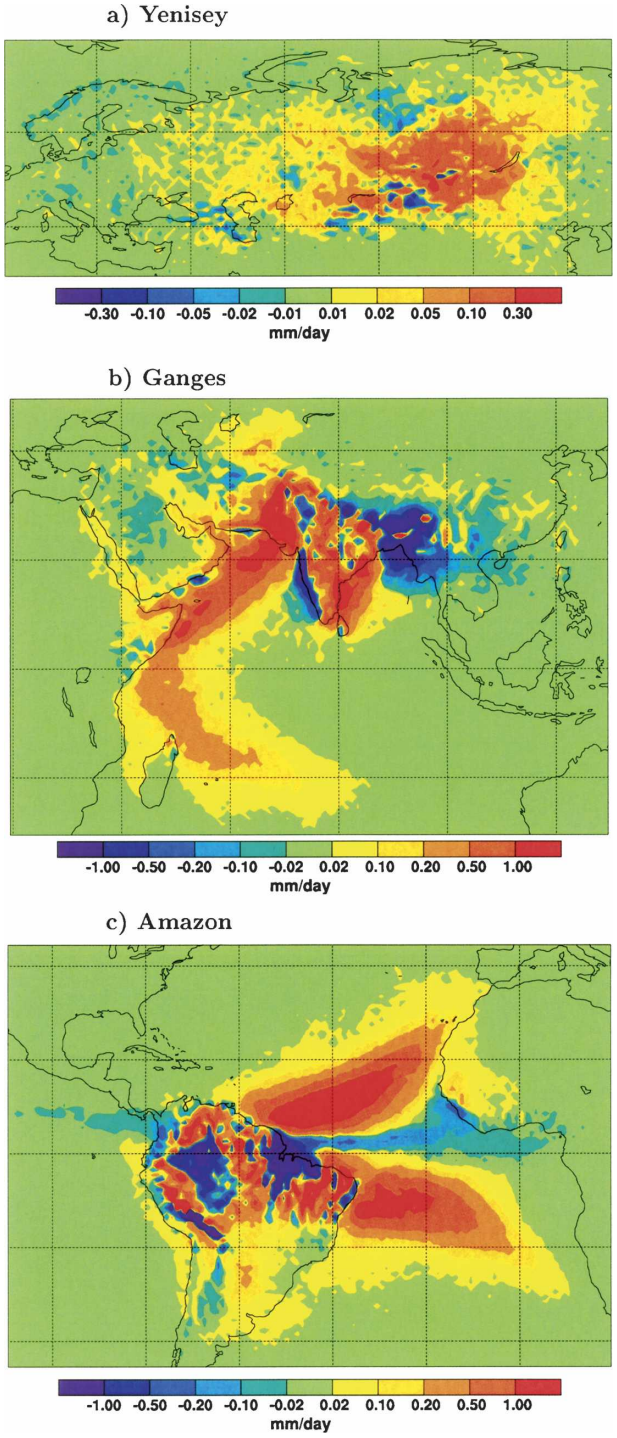

FIG. 11. Annual mean $(E - P)_c^{-10,i}$ fields from backward tracking for (a) the Yenisey, (b) the Ganges, and (c) the Amazon River.

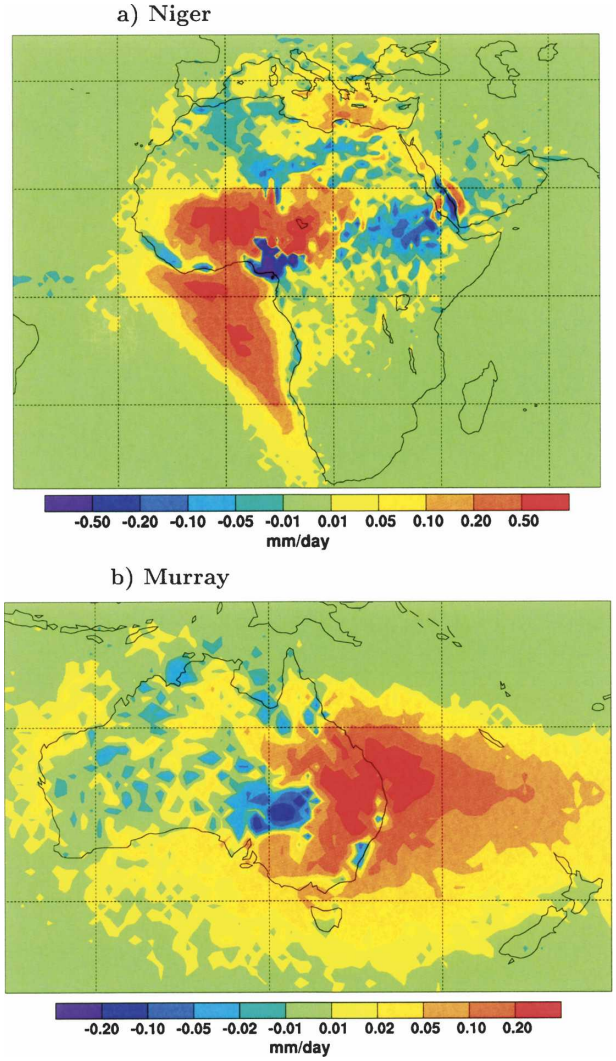

FIG. 12. Annual mean $(E - P)_c^{-10,i}$ fields from backward tracking for (a) the Niger and (b) the Murray River.

increase from $(E - P)_c^{-2,i} = -21\%$ to $(E - P)_c^{-10,i} = -3\%$, indicating that significant recycling may indeed take place, which is masked in the 10-day-integrated value by precipitation occurring shortly before an identified precipitation event. Eltahir and Bras (1996) reported recycling ratios of 25% and 35%, depending on the dataset used, and Trenberth (1999) reported various values from 5% to 34% for the Amazon basin, depending on how the recycling ratio was defined. Both studies also noted the large heterogeneity in the recycling ratio over the Amazon basin, a feature that is reflected also in our $(E - P)_c^{-10,i}$ field.

For the Murray River in Australia, the Pacific Ocean is the dominant moisture source (Table 4; Fig. 12b), but recycling over the basin and other parts of Australia also makes a significant contribution.

6. Discussion

In this paper and in Part I we have developed a Lagrangian method to track water vapor in the atmo-

sphere and diagnose its sources and sinks. There exist numerous other studies, many for extreme precipitation events, using trajectories for tracking water vapor (e.g., Wernli 1997; Dirmeyer and Brubaker 1999; Bertò et al. 2004; KM). While some of these methods are conceptually similar and have, in fact, inspired this work (e.g., Wernli 1997), none was applied on a global scale. Normal trajectory models start trajectories of a certain length from particular locations or from a regular grid. This makes them inefficient because the restarting interval must be shorter than the trajectory length, thus multiplying both the computation time and the size of the model output. With FLEXPART, in contrast, the atmosphere is divided into particles of equal mass that are then carried mass-consistently for periods that are limited only by the availability of the meteorological input data (to produce this climatology on a personal computer took only a few days). The model output is relatively compact (about 200 gigabytes for this study) and much smaller than what a conventional trajectory model would produce. This study was limited to transport times of 10 days, but the model output itself is suitable also for the analysis of much longer transport times, which would completely exhaust conventional trajectory models. Furthermore, FLEXPART contains parameterizations for turbulence (which were used here) and convection (which will be used in the future). We have used only q from the ECMWF data for our analysis, but the FLEXPART output could have been analyzed also with other methods, for instance by combining it with observed precipitation and forecast evaporation (e.g., Dirmeyer and Brubaker 1999). Thus, while the particle modeling approach has clear advantages over normal trajectory modeling, there appear to be no disadvantages.

The principal advantage of our method to diagnose $E - P$ is that it uses a single self-consistent meteorological analysis dataset and requires no additional input from observations or model forecasts. However, there are also two major disadvantages. First, the method diagnoses a flux quantity ($E - P$) using the time derivative of humidity along a particle trajectory. If the analysis data are noisy (i.e., contain unrealistic fluctuations of humidity), this will be diagnosed as moisture fluxes. If these errors are purely random, they would cancel each other for longer time averages. However, for shorter time periods or smaller regions, they could significantly affect our results.

Second, even though trajectory errors are random (Stohl 1998), they can affect the results systematically. Consider a particle that is originally located in a relatively moist air mass (e.g., over an ocean basin) that is tracked forward. If that particle leaves the tracked air mass because of trajectory errors and enters a drier air mass, q decreases along its trajectory, which erroneously leads to $(E - P)_c < 0$. Therefore, $(E - P)_c$ will be systematically too small for the forward tracking from moist regions. Trajectory accuracy is likely to be most critical for small basins and may be somewhat less critical for large basins. Second, the method as it was applied here cannot diagnose surface fluxes of moisture, but only the fluxes into or out of the tracked air mass. Considering again a moist air mass, it is likely that some of this moisture will be lost to other air masses via mixing and/or precipitation that reevaporates before reaching the surface. While the diagnosed moisture loss from the tracked air mass will be correct in this case, it will systematically overestimate the surface flux. The opposite problems occur if relatively dry air masses are tracked.

It is quite clear that our results are affected by these errors, as the moisture budget between forward and backward calculations is not closed. For instance, it was diagnosed that Mediterranean air masses supply about 9 times their precipitable water per year to the Danube basin (or at least to other air masses residing over that basin) (Table 3), which translates to a moisture loss of 300 $km^3\ yr^{-1}$ (400 $mm\ yr^{-1}$), about twice the unconditional $E - P$ for the Danube and more than half the annual precipitation. On the other hand, it was found that only 14% of the precipitation over the Danube was supplied directly via net evaporation over the Mediterranean (Table 4). While some of the discrepancy can be explained by the fact that Mediterranean air supplies moisture to drier air masses over the Danube basin (rather than to the surface), it is likely that the larger part of it comes from trajectory errors. More generally, it appears that the forward tracking overestimates both moisture losses over relatively dry regions and moisture gains over relatively moist regions. This will tend to enhance the $(E - P)_c$ patterns resulting from the forward tracking. Trajectory errors will likely affect the back tracking from the precipitation events much less as the moisture variability over the moisture source regions is less extreme than over the loss regions.

Because of the above problems, the results reported in Tables 3 and 4 should best be interpreted semiquantitatively only. The reported magnitudes of moisture sources and sinks tend to be overestimated; that is, they are too high for positive values and too small for negative ones. However, the general patterns of the $(E - P)_c$ fields and the relative ranking of moisture source and sink basins should be quite reliable as it is likely that trajectory errors will have similar effects over basins with similar characteristics. In the future, these errors could be reduced significantly by running a particle

model online with a data assimilation system. Using the full model resolution and the model-internal time steps would greatly help to reduce trajectory errors. Furthermore, if parameterizations for subgrid-scale processes (turbulence and convection) were consistent between the assimilating model and the particle model, errors in the $(E - P)_c$ budgets would be due solely to the assimilating model itself and the observations entering it.

The convection scheme in FLEXPART was not turned on in this study because, due to the model's offline nature, particles would fluctuate between drier and moister regions of the convective column and the moisture changes would be diagnosed as repeated changes in a particle's specific humidity. These fluctuations would be partly unrealistic, given that the moisture changes are diagnosed offline from the ECMWF model. While this would not affect $E - P$, it would affect the identification of significant precipitation events, the particle tracking, and $(E - P)_c$ budgets. In the future, the convection scheme will be turned on and particles undergoing convection will be marked, allowing one to test its effect. However, it is our experience from tracer studies (Stohl et al. 2002) that at the resolution used here simulated transport processes are relatively insensitive to whether the convection scheme is used or not. It is, thus, not expected that turning on the convection scheme would change the results significantly. Ideally, however, FLEXPART should be run online with the ECMWF model in order to use the convection scheme.

In this paper, we have studied only the mean conditions over the 4-yr period. In the future, however, the most interesting applications of this method will be to explore seasonal and interannual variability in the moisture transport, including extreme events (e.g., Brubaker et al. 2001). This could help to clarify the relation between climate variability and moisture transport. Comparing extremely wet seasons with drought periods could shed light onto the question how much of their difference is produced locally and how much is due to teleconnections, for instance, via different sea surface temperature distributions. An obvious advantage of this method compared to others in that regard is that it can be applied efficiently on a global scale and for long time periods.

There exist transport climatologies based on Lagrangian methods both for the atmosphere (Stohl 2001; Eckhardt et al. 2004) and for the oceans (Döös 1995; Blanke et al. 2001). Since evaporation and precipitation constitute a physical mass exchange between the two spheres, it would be quite interesting to develop a coupled climatology with the vision to trace water molecules through both the oceans and the atmosphere and identify source–sink relationships between them. In combination with a river transport model and land surface model, a truly global Lagrangian perspective of water transport could possibly be achieved. While such an undertaking would be considerable effort, this method could be the starting point.

7. Conclusions

The conclusions from this study are as follows:

- A Lagrangian particle dispersion model, driven with ECMWF analyses, has been used to calculate the trajectories of so-called particles, together representing the total mass of the atmosphere, over a 4-yr time period. The resulting dataset of specific humidity along trajectories can be used much more efficiently to study atmospheric transport processes than the trajectory methods used so far.
- The changes of specific humidity along the trajectories were used to diagnose net moisture loss or gains. It was shown that if all the particles in a column are considered, the method can diagnose budgets of evaporation minus precipitation ($E - P$) very accurately and consistently with existing Eulerian methods. The $E - P$ budgets for 39 river catchments worldwide were compared to climatological mean streamflow at the river mouths and it was found that for most of the world's largest rivers the two datasets agreed within about 20% (explained variance 87%).
- The method was then used to track moisture budgets forward from all ocean basins and backward from the 39 river catchments for a period of 10 days. For the backward tracking, only precipitating particles with a moisture loss in grid cells with significantly negative $E - P$ were considered in order to identify the moisture source of precipitation.
- The Atlantic Ocean and recycling over the North American continent were found to be the dominant moisture sources for precipitation over the Mississippi, in good quantitative agreement with previous trajectory studies (Dirmeyer and Brubaker 1999; Brubaker et al. 2001). In contrast to these studies but in good agreement with water tracer studies (Bosilovich and Schubert 2002; Bosilovich et al. 2003) the Pacific Ocean was not identified as a significant moisture source for Mississippi precipitation.
- Consistent with previous studies (e.g., Numaguti 1999) it was found that for 18 of the 39 river basins, more than 50% of the precipitation had its origin over land surfaces, most importantly for the rivers in northern Eurasia (Volga, Dnepr, Don, Ob, Yenisey, and Lena) that are remote from ocean basins.

- The source regions of water precipitated over the Ganges and Niger catchments stretch deeply into the Southern Hemisphere, due to the monsoon circulation, whereas the Amazon draws its precipitation from two separate source regions in the subtropics of both hemispheres.
- Transport of air from the North Pacific produces net evaporation over the North Atlantic, but not vice versa. Furthermore, transport of air from the Indian Ocean produces net precipitation over the Pacific. These differences are an important reason why the North Atlantic is more saline than the North Pacific, and, thus, why deep ocean water forms only in the North Atlantic. This is further supported by much less atmospheric moisture transport into the Arctic Ocean than into the Southern Ocean.
- Trajectory errors lead to systematic effects in the tracked ($E - P$) budgets. Running the dispersion model online with a data assimilation system could reduce these errors significantly and would improve the accuracy of the tracked ($E - P$) budgets.

Acknowledgments. ECMWF and the German Weather Service are acknowledged for permitting access to the ECMWF archives. The insightful comments of three reviewers contributed to shape the final version of this paper.

REFERENCES

Bertò, A., A. Buzzi, and D. Zardi, 2004: Back-tracking water vapour contributing to a precipitation event over Trentino: A case study. *Meteor. Z.,* **13,** 189–200.

Betts, A. K., J. H. Ball, and P. Viterbo, 2003: Evaluation of the ERA-40 surface water budget and surface temperature for the Mackenzie River basin. *J. Hydrometeor.,* **4,** 1194–1211.

Blanke, B., S. Speich, G. Madec, and K. Döös, 2001: A global diagnostic of interocean mass transfers. *J. Phys. Oceanogr.,* **31,** 1623–1632.

Bosilovich, M. G., and S. D. Schubert, 2002: Water vapor tracers as diagnostics of the regional hydrological cycle. *J. Hydrometeor.,* **3,** 149–165.

——, Y. C. Sud, S. D. Schubert, and G. K. Walker, 2003: Numerical simulation of the large-scale North American monsoon water sources. *J. Geophys. Res.,* **108,** 8614, doi:10.1029/2002JD003095.

Brubaker, K. L., D. Entekhabi, and P. S. Eagleson, 1993: Estimation of continental precipitation recycling. *J. Climate,* **6,** 1077–1089.

——, P. A. Dirmeyer, A. Sudradjat, B. S. Levy, and F. Bernal, 2001: A 36-yr climatological description of the evaporative sources of warm-season precipitation in the Mississippi River basin. *J. Hydrometeor.,* **2,** 537–557.

Chen, T.-C., J. Pfaendtner, and S.-P. Weng, 1994: Aspects of the hydrological cycle of the ocean–atmosphere system. *J. Phys. Oceanogr.,* **24,** 1827–1833.

Conkright, M. E., R. A. Locarnini, H. E. Garcia, T. D. O'Brien, T. P. Boyer, C. Stephens, and J. I. Antonov, 2002: World Ocean Atlas 2001: Objective analyses, data statistics, and figures. CD-ROM documentation. National Oceanographic Data Center Internal Rep. 17, 21 pp.

Crimp, S. J., and S. J. Mason, 1999: The extreme precipitation event of 11 to 16 February 1996 over South Africa. *Meteor. Atmos. Phys.,* **70,** 29–42.

D'Abreton, P. C., and P. D. Tyson, 1996: Three-dimensional kinematic trajectory modelling of water vapour transport over southern Africa. *Water SA,* **22,** 297–306.

Dai, A., and K. E. Trenberth, 2002: Estimates of freshwater discharge from continents: Latitudinal and seasonal variations. *J. Hydrometeor.,* **3,** 660–687.

Dirmeyer, P. A., and K. L. Brubaker, 1999: Contrasting evaporative moisture sources during the drought of 1988 and the flood of 1993. *J. Geophys. Res.,* **104,** 19 383–19 397.

Döös, K., 1995: Interocean exchange of water masses. *J. Geophys. Res.,* **100,** 13 499–13 514.

Eckhardt, S., A. Stohl, H. Wernli, P. James, C. Forster, and N. Spichtinger, 2004: A 15-year climatology of warm conveyor belts. *J. Climate,* **17,** 218–237.

Eltahir, E. A. B., and R. L. Bras, 1996: Precipitation recycling. *Rev. Geophys.,* **34,** 367–378.

Emile-Geay, J., M. A. Cane, N. Naik, R. Seager, A. C. Clement, and A. van Geen, 2003: Warren revisited: Atmospheric freshwater fluxes and why is no deep water formed in the North Pacific. *J. Geophys. Res.,* **108,** 3178, doi:10.1029/2001JC001058.

Fekete, B. M., C. J. Vörösmarty, and W. Grabs, 2000: Global composite runoff fields based on observed river discharge and simulated water balances. Global Runoff Data Centre Rep. 22, Koblenz, Germany, 39 pp. plus annex. [Available online at http://www.grdc.sr.unh.edu.]

Fukutomi, Y., H. Igarashi, K. Masuda, and T. Yasunari, 2003: Interannual variability of summer water balance components in three major river basins of northern Eurasia. *J. Hydrometeor.,* **4,** 283–296.

Godfred-Spenning, C. R., and C. J. C. Reason, 2002: Interannual variability of lower-tropospheric moisture transport during the Australian monsoon. *Int. J. Climatol.,* **22,** 509–532.

Gong, C., and E. Eltahir, 1996: Sources of moisture for rainfall in West Africa. *Water Resour. Res.,* **32,** 3115–3121.

Gutowski, W. J., Jr., Y. Chen, and Z. Ötles, 1997: Atmospheric water vapor transport in NCEP–NCAR reanalyses: Comparison with river discharge in the central United States. *Bull. Amer. Meteor. Soc.,* **78,** 1957–1969.

Hasumi, H., 2002: Sensitivity of the global thermohaline circulation to interbasin freshwater transport by the atmosphere and the Bering Strait throughflow. *J. Climate,* **15,** 2516–2526.

Hung, C.-W., and M. Yanai, 2004: Factors contributing to the onset of the Australian summer monsoon. *Quart. J. Roy. Meteor. Soc.,* **130,** 739–758.

Knippertz, P., and J. E. Martin, 2005: Tropical plumes and extreme precipitation in subtropical and tropical West Africa: Part 1. Moisture transport and precipitation generation. *Quart. J. Roy. Meteor. Soc.,* **131,** 2337–2365.

Koster, R., and Coauthors, 1986: Global sources of local precipitation as determined by the NASA/GISS GCM. *Geophys. Res. Lett.,* **13,** 121–124.

Liu, J., and R. E. Stewart, 2003: Water vapor fluxes over the Saskatchewan River basin. *J. Hydrometeor.,* **4,** 944–959.

Numaguti, A., 1999: Origin and recycling processes of precipitating water over the Eurasian continent: Experiments using an

atmospheric general circulation model. *J. Geophys. Res.,* **104,** 1957–1972.

Rasmusson, E. M., 1968: Atmospheric water vapor transport and the water balance of North America. II. Large-scale water balance investigations. *Mon. Wea. Rev.,* **96,** 720–734.

Roads, J., and Coauthors, 2003: GCIP water and energy budget synthesis (WEBS). *J. Geophys. Res.,* **108,** 8609, doi:10.1029/2002JD002583.

Seneviratne, S., P. Viterbo, D. Lüthi, and C. Schär, 2004: Inferring changes in terrestrial water storage using ERA-40 reanalysis data: The Mississippi River basin. *J. Climate,* **17,** 2039–2057.

Serreze, M. C., and A. J. Etringer, 2003: Precipitation characteristics of the Eurasian Arctic drainage system. *Int. J. Climatol,* **23,** 1267–1291.

——, D. H. Bromwich, M. P. Clark, A. J. Etringer, T. Zhang, and R. Lammers, 2002: Large-scale hydro-climatology of the terrestrial Arctic drainage system. *J. Geophys. Res.,* **108,** 8160, doi:10.1029/2001JD000919.

Smirnov, V. V., and G. W. K. Moore, 2001: Short-term and seasonal variability of the atmospheric water vapor transport through the Mackenzie River basin. *J. Hydrometeor.,* **2,** 441–452.

Stohl, A., 1998: Computation, accuracy and applications of trajectories—A review and bibliography. *Atmos. Environ.,* **32,** 947–966.

——, 2001: A 1-year Lagrangian climatology of airstreams in the Northern Hemisphere troposphere and lowermost stratosphere. *J. Geophys. Res.,* **106,** 7263–7279.

——, and P. James, 2004: A Lagrangian analysis of the atmospheric branch of the global water cycle. Part 1: Method description, validation, and demonstration for the August 2002 flooding in central Europe. *J. Hydrometeor.,* **5,** 656–678.

——, M. Hittenberger, and G. Wotawa, 1998: Validation of the Lagrangian particle dispersion model FLEXPART against large scale tracer experiment data. *Atmos. Environ.,* **32,** 4245–4264.

——, S. Eckhardt, C. Forster, P. James, and N. Spichtinger, 2002: On the pathways and timescales of intercontinental air pollution transport. *J. Geophys. Res.,* **107,** 4684, doi:10.1029/2001JD001396.

Trenberth, K. E., 1997: Using atmospheric budgets as a constraint on surface fluxes. *J. Climate,* **10,** 2796–2809.

——, 1999: Atmospheric moisture recycling: Role of advection and local evaporation. *J. Climate,* **12,** 1368–1381.

——, and C. J. Guillemot, 1998: Evaluation of the atmospheric moisture and hydrological cycle in the NCEP/NCAR reanalysis. *Climate Dyn.,* **14,** 213–231.

Vörösmarty, C. J., B. M. Fekete, M. Meybeck, and B. Lammers, 2000: Global system of rivers: Its role in organizing continental land mass and defining land-to-ocean linkages. *Global Biogeochem. Cycles,* **14,** 599–621.

Weaver, A. J., C. M. Bitz, A. F. Fanning, and M. M. Holland, 1999: Thermohaline circulation: High-latitude phenomena and the difference between the Pacific and Atlantic. *Annu. Rev. Earth Planet. Sci.,* **27,** 231–285.

Webster, P. J., 1994: The role of hydrological processes in ocean–atmosphere interactions. *Rev. Geophys.,* **32,** 427–476.

Wernli, H., 1997: A Lagrangian-based analysis of extratropical cyclones. II: A detailed case-study. *Quart. J. Roy. Meteor. Soc.,* **123,** 1677–1706.

White, P. W., Ed., 2002: IFS documentation. ECMWF Rep., Reading, United Kingdom. [Available online at http://www.ecmwf.int.]